© 2018. Published by The Company of Biologists Ltd | Development (2018) 145, dev154054. doi:10.1242/dev.154054

RESEARCH ARTICLE

The G protein-coupled receptor Gpr161 regulates forelimb formation, limb patterning and skeletal morphogenesis in a primary cilium-dependent manner

Sun-hee Hwang[1], Kevin A. White[2], Bandarigoda N. Somatilaka[1], John M. Shelton[2], James A. Richardson[3] and Saikat Mukhopadhyay[1,*]

ABSTRACT

The role of basal suppression of the sonic hedgehog (Shh) pathway and its interaction with Indian hedgehog (Ihh) signaling during limb/skeletal morphogenesis is not well understood. The orphan G protein-coupled receptor Gpr161 localizes to primary cilia and functions as a negative regulator of Shh signaling by promoting Gli transcriptional repressor versus activator formation. Here, we show that forelimb buds are not formed in *Gpr161* knockout mouse embryos despite establishment of prospective limb fields. Limb-specific deletion of *Gpr161* resulted in prematurely expanded Shh signaling and ectopic Shh-dependent patterning defects resulting in polysyndactyly. In addition, endochondral bone formation in forearms, including formation of both trabecular bone and bone collar was prevented. Endochondral bone formation defects resulted from accumulation of proliferating round/periarticular-like chondrocytes, lack of differentiation into columnar chondrocytes, and corresponding absence of Ihh signaling. *Gpr161* deficiency in craniofacial mesenchyme also prevented intramembranous bone formation in calvarium. Defects in limb patterning, endochondral and intramembranous skeletal morphogenesis were suppressed in the absence of cilia. Overall, Gpr161 promotes forelimb formation, regulates limb patterning, prevents periarticular chondrocyte proliferation and drives osteoblastogenesis in intramembranous bones in a cilium-dependent manner.

KEY WORDS: Primary cilia, G protein-coupled receptor, Hedgehog, Endochondral bone, Intramembranous bone, Limb

INTRODUCTION

Limb development is an orchestrated process involving initiation of the limb bud from the lateral plate mesoderm (Gros and Tabin, 2014; Duboc and Logan, 2011), patterning of the limb bud (Zeller et al., 2009), and skeletal morphogenesis (Kronenberg, 2003). Sonic hedgehog (Shh) and Indian hedgehog (Ihh) are crucial factors in limb and skeletal development, but they have distinct functions in these processes. Shh expression starts in the posterior forelimb bud from embryonic day (E) 9.5 (Platt et al., 1997; Lewis et al., 2001) and continues until E12 to regulate limb bud patterning (Zeller et al., 2009). In contrast, Ihh is secreted from pre-hypertrophic and hypertrophic chondrocytes starting at E11.5 (Bitgood and McMahon, 1995) and regulates endochondral bone formation (Long et al., 2004; St-Jacques et al., 1999; Lanske et al., 1996; Vortkamp et al., 1996). Ihh also inhibits early stages of osteoblast differentiation during intramembranous bone formation (Abzhanov et al., 2007). Shh- and Ihh-mediated activation in limb and skeletal morphogenesis has been studied extensively (Mak et al., 2006; Kobayashi et al., 2005; Butterfield et al., 2009). However, the role of suppression of these morphogenetic pathways beyond the periods of expression of Shh/Ihh is underappreciated.

The primary cilium is a microtubule-based dynamic cellular appendage that mediates extracellular signaling particularly with respect to vertebrate Shh signaling (Goetz and Anderson, 2010). Activation of the Shh pathway by formation of the Gli transcriptional activator (GliA) and basal repression of the pathway by Gli transcriptional repressor (GliR) are both dependent on the primary cilium (Goetz and Anderson, 2010). Binding of Shh to patched 1 (Ptch1) triggers removal of Ptch1 from cilia, and promotes smoothened (Smo) enrichment in cilia, which mediates GliA formation (Corbit et al., 2005; Rohatgi et al., 2007). In contrast, the basal repression machinery of Shh signaling involves protein kinase A (PKA)-mediated GliR formation in a cilia-dependent manner (Mukhopadhyay and Rohatgi, 2014).

We recently described that the cilia-localized orphan G protein-coupled receptor (GPCR) Gpr161 functions as a negative regulator of Shh signaling during early neural tube development in mice (Mukhopadhyay et al., 2013). *Gpr161* knockout results in increased Shh signaling (ventralization) throughout the rostrocaudal extent of the neural tube, without disrupting cilia. Gpr161 determines Gli3R formation possibly via constitutive cAMP signaling. Another negative regulator, suppressor of fused (Sufu), restrains Gli3 in cytoplasm and promotes Gli3R processing (Humke et al., 2010) in a cilia-independent step (Jia et al., 2009). Importantly, lack of Gpr161-, PKA- and Sufu-dependent basal suppression cause high Shh signaling during mouse neural tube development (Tuson et al., 2011; Mukhopadhyay et al., 2013; Svärd et al., 2006), similar to *Ptch1* knockout, which results in activation of the canonical Smo-dependent arm of the pathway (Goodrich et al., 1997). Thus, both transcriptional activation and basal repression mechanisms are crucial for regulation of high Shh signaling.

In addition to Gpr161, we and other groups have recently described other important factors in the basal repression machinery of Shh signaling. Typically, mutants that disrupt cilia, such as those affecting the intraflagellar transport-B (IFT-B) complex, cause low Shh signaling in the neural tube (Goetz and Anderson, 2010; Huangfu et al., 2003). Paradoxically, mutations in the IFT-A complex subunits, despite having bulbous ciliary tips caused by defective retrograde IFT (Liem et al., 2012; Ocbina et al., 2011; Qin

[1]Department of Cell Biology, UT Southwestern Medical Center, Dallas, Texas, USA. [2]Internal Medicine, UT Southwestern Medical Center, Dallas, Texas, USA. [3]Pathology, UT Southwestern Medical Center, Dallas, Texas, USA.

*Author for correspondence (Saikat.Mukhopadhyay@utsouthwestern.edu)

S.M., 0000-0003-4790-3090

Received 3 May 2017; Accepted 22 November 2017

Development (2018) 145, dev154054. doi:10.1242/dev.154054

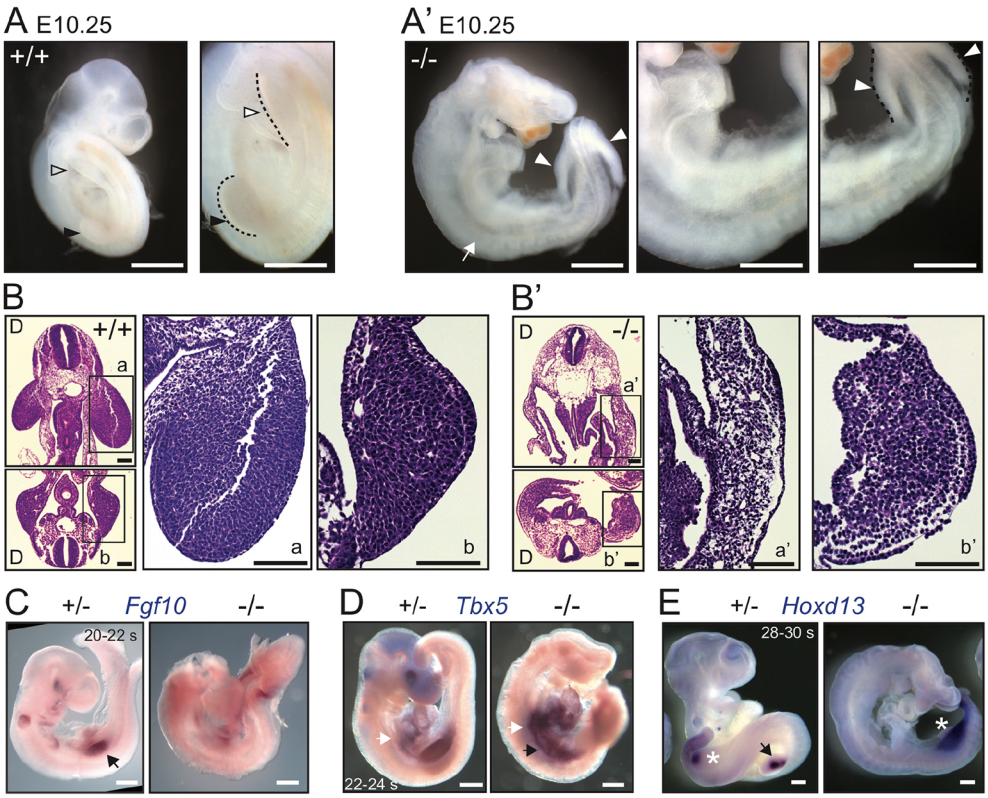

Fig. 1. *Gpr161* knockouts lack forelimbs. (A,A′) Lateral views and corresponding insets of E10.25 embryos showing lack of forelimb buds with presence of hindlimb buds in *Gpr161* knockout (–/–) versus wild type (+/+). Black arrowheads and white arrowheads mark forelimb and hindlimb, respectively. White arrow marks absent forelimb. *n*=51 (+/+ or +/–) and 21 (–/–) embryos. (B,B′) Hematoxylin and Eosin-stained horizontal sections of E10.25 embryos at the level of forelimbs (top) and hindlimbs (bottom) with corresponding enlarged views for wild type (+/+; a,b) and *Gpr161*$^{-/-}$ (a′-b′) show lack of forelimb mesenchyme in knockout. D marks the dorsal side. Also see Movies 1-4. *n*=3 embryos each. (C) Whole-mount digoxigenin-labeled RNA *in situ* hybridization for *Fgf10* shows expression in the forelimb bud (arrow) in heterozygote (+/–) littermate embryos at E9.25, whereas expression is absent in the prospective forelimb region of *Gpr161*$^{-/-}$ embryos. *n*=2 embryos each. (D) RNA *in situ* hybridization for *Tbx5* shows expression at the level of the heart (white arrows) and prospective forelimb fields (black arrows) at ∼E9.5 in *Gpr161*$^{-/-}$ embryos whereas it is expressed in forelimb in heterozygote littermate (+/–). *n*=3 embryos (control), 2 embryos (knockout). (E) RNA *in situ* hybridization shows expression of *Hoxd13* in posterior forelimb and hindlimb buds in heterozygote (+/–) littermate embryo, whereas expression is absent in *Gpr161*$^{-/-}$ in forelimb region and present diffusely in the hindlimb buds at ∼E10.25. Black arrows and white asterisks depict forelimb and hindlimb, respectively. *n*=2 embryos each. Somite counts of control littermate embryos in C-E were used to determine gestational ages. s, somite. Scale bars: 1 mm (A,A′); 100 µm (B,B′); 500 µm (C-E). See also Fig. S1.

et al., 2011; Tran et al., 2008), result in increased Shh signaling in the neural tube. Interestingly, mutations in the tubby-like protein 3 gene (*Tulp3*) phenocopy mutations in IFT-A subunits and *Gpr161* by causing increased Shh signaling in the caudal neural tube (Norman et al., 2009; Patterson et al., 2009). The pre-ciliary function of the IFT-A core complex in binding and ciliary trafficking of Tulp3, an adapter in gating of ciliary GPCRs including Gpr161, explains the high Shh signaling observed in IFT-A mutants, despite having abnormal cilia (Badgandi et al., 2017; Mukhopadhyay et al., 2013, 2010). Thus, IFT-A-regulated trafficking of Tulp3 and Gpr161 regulates basal suppression of Shh signaling.

During limb and skeletal development, mesenchymal cells of the limb bud, perichondrial cells, chondrocytes, osteoblasts and osteocytes are ciliated (Donnelly et al., 2008; Farnum and Wilsman, 2011; Haycraft et al., 2007; Malone et al., 2007; Xiao et al., 2006; Wilsman et al., 1980). A subset of diseases caused by primary cilia/centrosome defects (ciliopathies) are associated with skeletal phenotypes, and classified as skeletal ciliopathies, highlighting the role of cilia in limb and skeletal development. These diseases include Sensenbrenner syndrome, Jeune syndrome or asphyxiating thoracic dystrophy (ATD), and the short rib-polydactyly group (SRPs) (Huber and Cormier-Daire, 2012). Particularly, mutations in the IFT-A complex have been associated predominantly with Sensenbrenner syndrome, a syndrome with craniofacial and ectodermal abnormalities that are distinct from other skeletal ciliopathies (Lin et al., 2013). Tissue-specific deletion of *Sufu* in mice increases Shh signaling in limb bud and cranial mesenchyme, affecting limb patterning (Zhulyn et al., 2014) and preventing intramembranous bone formation in skull (Li et al., 2017), respectively. However, the role of cilia in repression of Shh signaling and in causing distinct phenotypic characteristics of skeletal ciliopathies is not well understood.

Here, we show that Gpr161 regulates forelimb formation and Shh-dependent limb bud patterning, as well as endochondral and intramembranous bone formation in a cilia-dependent manner. Our results demonstrate an unexpected and crucial role played by the cilia in basally repressing the hedgehog pathway in these developmental processes, even at times when the activating morphogen is absent.

RESULTS

Generation of a conditional knockout *Gpr161* allele in mice

To study the role of Gpr161 during different stages of limb and skeletal development, we generated a mouse allele floxed on both sides of exon 4 (*Gpr161*$^{f/f}$) (Fig. S1A). We determined that embryos

Development (2018) 145, dev154054. doi:10.1242/dev.154054

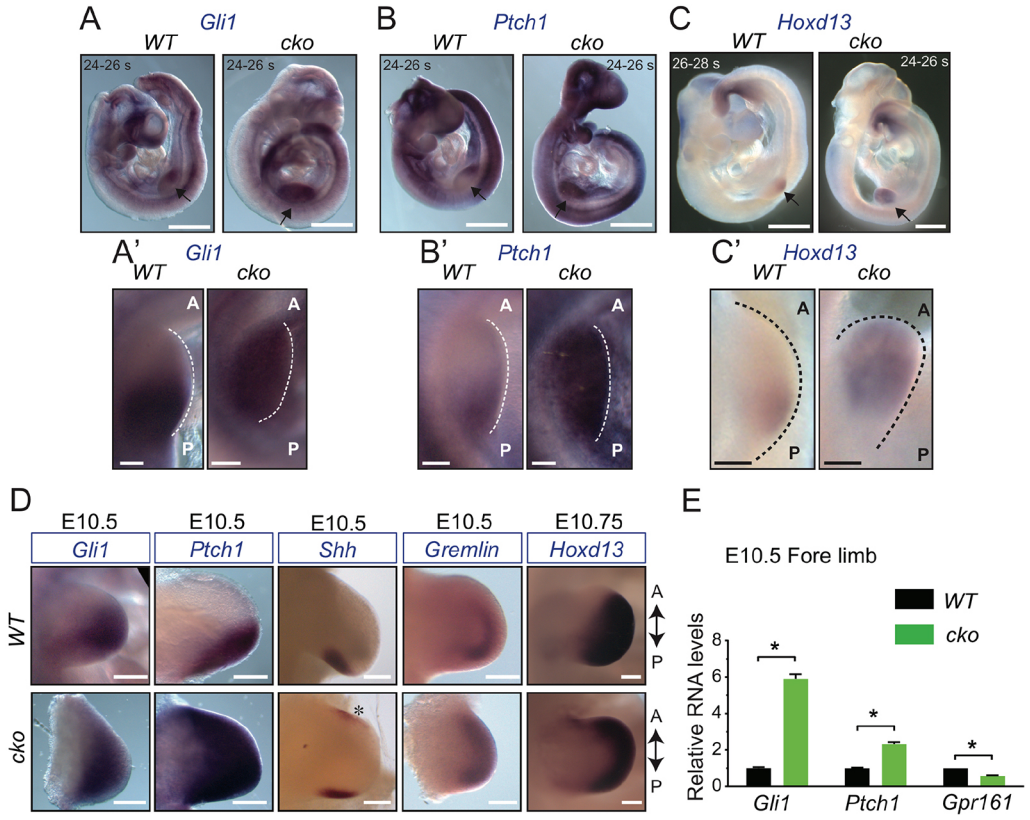

Fig. 2. *Gpr161* knockouts exhibit high Shh pathway activity. (A-C′) Lateral views of RNA *in situ* hybridization for *Gli1* (A), *Ptch1* (B) and *Hoxd13* (C) in *Prx1-Cre; Gpr161*$^{f/f}$ (cko) embryos show increased expression throughout forelimb buds with respect to *Prx1-Cre; Gpr161*$^{fl/+}$ (WT) at ∼E9.5. Forelimb buds are marked by black arrows and are shown magnified in A′-C′, oriented in anterior (A)-posterior (P) axis. s, somite. *n*=4 limb buds each. (D) RNA *in situ* hybridization for *Gli1* and *Ptch1* in *Prx1-Cre; Gpr161*$^{f/f}$ (cko) versus *Prx1-Cre; Gpr161*$^{fl/+}$ (WT) forelimb buds show increased expression at E10.5 (*n*=4 limb buds each). *Shh* shows ectopic expression anteriorly (asterisk) in forelimb buds in cko embryos (*n*=6 limb buds each). *Grem1* expression is extended anteriorly in cko embryos (*n*=2 limb buds in WT, 4 in cko). By E10.75, *Hoxd13* expression is anteriorly expanded in forelimb buds in cko (*n*=2 limb buds each). (E) qRT-PCR of designated transcripts normalized to *Rpl19* in forelimb regions of E10.5 *Prx1-Cre; Gpr161*$^{f/f}$ (cko) versus *Prx1-Cre; Gpr161*$^{fl/+}$ (WT). *n*=3 limb buds each. **P*<0.0001 by *t*-test. Error bars represent s.d. Scale bars: 500 µm (A-C); 100 µm (A′-C′); 200 µm (D). See also Fig. S2.

homozygous for global deletion using this allele (*Gpr161*$^{-/-}$) were lethal by E10.5, had craniofacial defects (Fig. 1A,A′), neural tube ventralization (Fig. S1B), increased Shh signaling, and decreased Gli3R levels in E9.5 whole embryo lysates (Fig. S1C), similar to the previous null allele targeting exon 3 (Mukhopadhyay et al., 2013). Thus, the present allele is a null allele, and the conditional form of the allele can be used to study tissue-specific phenotypes.

Gpr161 knockout lacks forelimbs

Gpr161 is broadly expressed in the limb buds (Mukhopadhyay et al., 2013), and is localized to primary cilia of forelimb bud mesenchymal cells (Fig. S1D). Interestingly, by E10.25, *Gpr161*$^{-/-}$ embryos exhibited complete lack of forelimb buds, despite development of hindlimb buds (Fig. 1A,A′, Fig. S1E). Histological analysis confirmed the absence and presence of forelimb and hindlimb buds, respectively (Fig. 1B,B′, Movies 1-4). Expression of the fibroblast growth factor family gene *Fgf10* is initially restricted in the lateral plate mesoderm destined to become forelimb (prospective forelimb field), and observed later in the distal mesenchyme of the forelimb bud (Ohuchi et al., 1997; Agarwal et al., 2003; Rallis et al., 2003). At E9.25, *Fgf10* was not expressed in the prospective forelimb field of *Gpr161*$^{-/-}$ embryos, but was expressed in forelimb buds of littermate controls (Fig. 1C). The T-box transcription factor *Tbx5* is expressed in the prospective forelimb field prior to *Fgf10*, and is later expressed in the developing forelimb bud (Agarwal et al., 2003; Rallis et al., 2003; Sekine et al., 1999). At ∼E9.5, although forelimb buds were absent in *Gpr161*$^{-/-}$ embryos, *Tbx5* was expressed in the prospective forelimb field (Fig. 1D), unlike *Fgf10* (Fig. 1C), and was expressed in forelimb buds of littermate controls (Fig. 1D). In contrast, *Hoxd13* expression was evident in the hindlimb buds at E10.25, although its expression was broad and diffuse in contrast to tight posterior expression in littermate controls (Fig. 1E). Thus, knockout of *Gpr161* results in lack of forelimb, despite establishment of a *Tbx5*-expressing prospective forelimb field.

Gpr161 knockouts exhibit high Shh pathway activity

To test the role of Gpr161 during limb bud development, we conditionally deleted *Gpr161* using *Prx1-Cre*. Expression of *Prx1-Cre* is initiated in the prospective forelimb field (Hasson et al., 2007) following *Tbx5* (Nishimoto et al., 2015; Minguillon et al., 2012), with later expression in both forelimb and hindlimb mesenchyme (Logan et al., 2002). Unlike *Gpr161*$^{-/-}$, conditional deletion of *Gpr161* in forelimb fields using *Prx1-Cre* (*Prx1-Cre; Gpr161*$^{f/f}$, and hereafter designated as '*Gpr161* cko') did not cause defective limb formation, presumably resulting from later depletion of *Gpr161* in the prospective limb field compared with the knockout.

Prior to Shh expression in the posterior forelimb bud at E9.5, mutual antagonism between Gli3R and the basic helix-loop-helix transcription factor dHand (Hand2) prepatterns the forelimb mesenchyme to cause

Development (2018) 145, dev154054. doi:10.1242/dev.154054

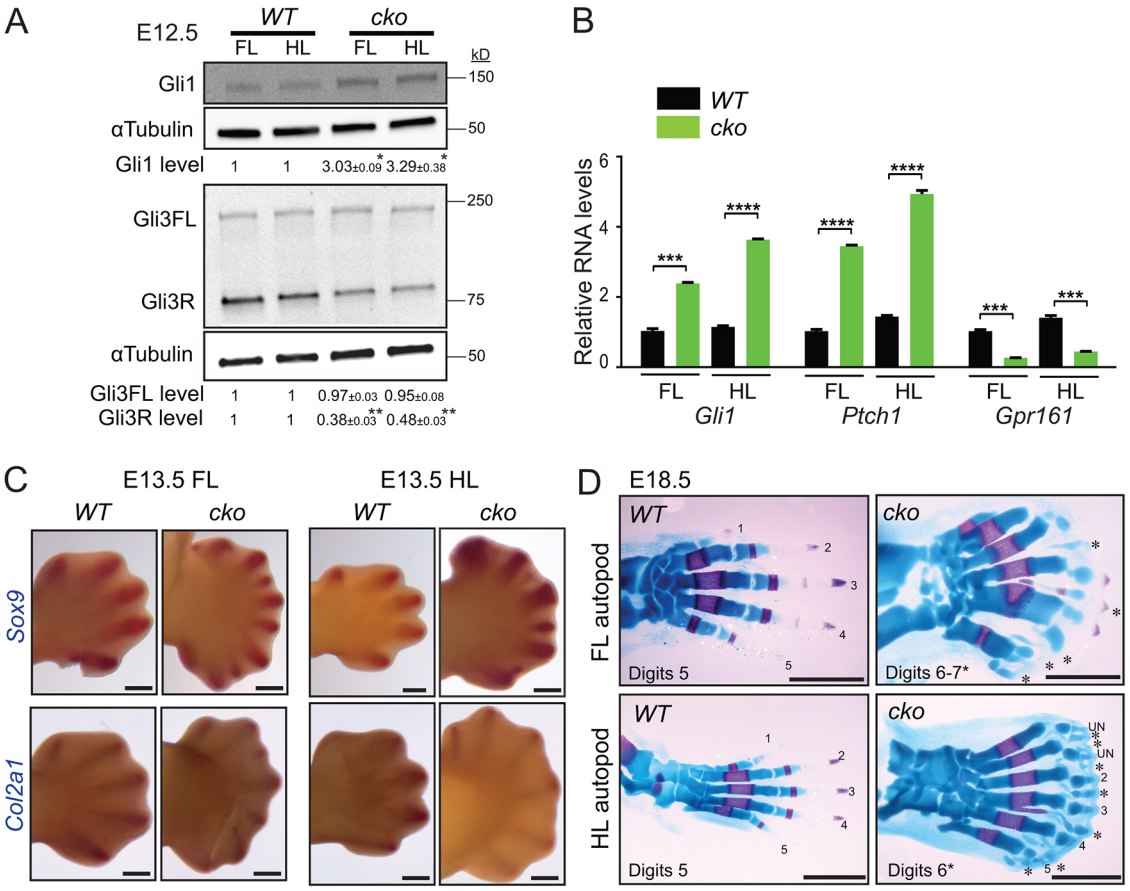

Fig. 3. High Shh signaling in *Gpr161* conditional knockout disrupts limb patterning. (A) Immunoblotting of forelimb (FL) and hindlimb (HL) buds shows increased levels of Gli1 and decreased Gli3R levels in E12.5 *Prx1-Cre; Gpr161$^{fl/f}$* (cko) versus *Prx1-Cre; Gpr161$^{fl/+}$* (WT), both of which were normalized to α-tubulin. For Gli1, *n*=2 experiments; for Gli3, *n*=3 experiments. Data represent mean±s.d. *P<0.05, **P<0.01 by *t*-test with respect to corresponding WT. (B) qRT-PCR of designated transcripts normalized to *Rpl19* in forelimb (FL) and hindlimb (HL) regions of E12.5 embryos in *Prx1-cre; Gpr161$^{fl/f}$* (cko) versus *Prx1-cre; Gpr161$^{fl/+}$* (WT). *n*=3 limbs each. ***P<0.001, ****P<0.0001 by *t*-test. Error bars represent s.d. (C) RNA *in situ* hybridization for *Sox9* and *Col2a1* in E13.5 *Prx1-Cre; Gpr161$^{fl/f}$* (cko) versus *Prx1-Cre; Gpr161$^{fl/+}$* (WT) in forelimbs and hindlimbs show increased mesenchymal/chondrogenic condensations in *Gpr161* cko. Digit field numbers were eight to ten in cko forelimbs and six to eight in cko hind limbs. *n*=4 limb buds each. (D) Alcian Blue (unmineralized cartilage) and Alizarin Red (mineralized cartilage and bone) staining of autopods in E18.5 *Prx1-Cre; Gpr161$^{fl/+}$* (WT) (*n*=36), *Prx1-Cre; Gpr161$^{fl/f}$* (cko) (*n*=20). Main digit numbers [excluding metacarpal bifurcations or duplicated/triplicated phalanges (asterisks)] and identities, wherever possible, have been designated. UN, unassigned digits. In *Gpr161* cko autopod, the predominant digit count is six, with rarely seen seven digits. Note lack of digit 1, syndactyly, bifurcated middle metacarpal, and duplicated/triplicated phalanges in the cko forelimb autopod. Note lack of digit 1 (lack of medial cuneiform), bifurcated third metatarsal, and duplicated/triplicated phalanges in the cko feet. Scale bars: 500 µm (C); 1 mm (D).

posterior expression of bona fide Shh pathway targets and of 5′ Hoxd genes such as *Hoxd13* (Te Welscher et al., 2002a). Interestingly, although *Gli3* transcript levels were unchanged (Fig. S2A), consistent with a lack of Gli3R protein activity, *Gli1*, *Ptch1* and *Hoxd13* expression was expanded throughout the *Gpr161* cko forelimb buds, in contrast to restricted posterior expression in littermate controls at ∼E9.5 (Fig. 2A-C′). Thus, *Gpr161* knockouts exhibit prematurely expanded Shh signaling.

As *Gpr161* cko demonstrated prematurely high signaling prior to Shh expression, we tested for pathway activity and limb bud patterning in *Gpr161* cko after Shh expression at E9.5. By E10.5, *Gpr161* cko embryos demonstrated (1) ectopic *Shh* expression in anterior forelimb field (Fig. 2D), (2) increased expression of *Gli1* and *Ptch1* in both anterior and posterior forelimb fields, as opposed to mainly posterior field expression in control littermates (Fig. 2D), (3) increased *Gli1* and *Ptch1* transcripts in the forelimbs compared with control littermates despite partial (∼50%) knockdown of *Gpr161* transcripts (Fig. 2E), suggestive of increased Shh signaling, and (4) extended expression of the bone morphogenetic protein antagonist *Grem1* and *Hoxd13* into anterior limb fields (Fig. 2D) (Te Welscher et al., 2002b; Zeller et al., 2009). Patterning of the hindlimbs in *Gpr161* cko was not affected until E10.5, but hindlimbs exhibited *Hoxd13* expansion anteriorly by E10.75 (Fig. S2B). Similar to *Gpr161* cko, the *Prx1-Cre*; *Ptch1* conditional knockout embryos also exhibit increased Shh signaling, although forelimbs are severely stunted, and hindlimbs manifest patterning defects (Butterfield et al., 2009; Zhulyn et al., 2014). Thus, limb-specific deletion of *Gpr161* resulted in prematurely expanded Shh signaling- and ectopic Shh-dependent patterning defects.

High Shh signaling in *Gpr161* conditional knockout results in polysyndactyly

Coincident with the increased Shh signaling and lack of Gli3R that persisted into E12.5 (Fig. 3A,B), E13.5 *Gpr161* cko embryos had an increased number of mesenchymal and chondrogenic condensations, resulting in an increased number of digit fields (Fig. 3C). During later embryonic development, we detected syndactyly, extra middle digits

Development (2018) 145, dev154054. doi:10.1242/dev.154054

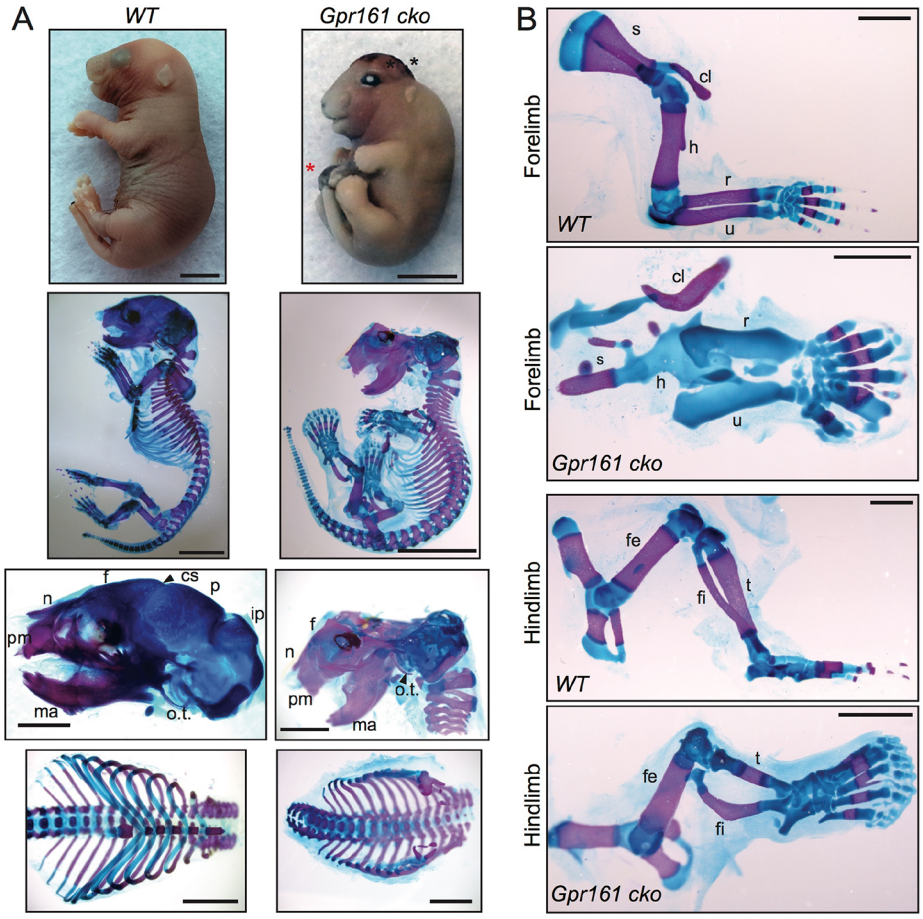

Fig. 4. Gpr161 determines endochondral and intramembranous bone formation.
(A,B) Whole embryo gross features (top, lateral view), and Alcian Blue (unmineralized cartilage) and Alizarin Red (mineralized cartilage and bone) staining of full skeleton (second row, lateral view), cranium (third row, lateral view), rib cage (bottom row, frontal view) (A), and forelimbs and hindlimbs (lateral view) (B) in E18.5 *Prx1-Cre; Gpr161*$^{fl/+}$ (WT) and *Prx1-Cre; Gpr161*$^{fl/f}$ (*Gpr161* cko) embryos. Black and red asterisks denote cranial and anterior thoracic/abdominal wall defects, respectively. In *Gpr161* cko, the posterior calvarium and most of the scapula were lacking in mineralization. The ribcage was lacking in sternum and the ventral ribs were not fused and widely open. In addition, there was no endochondral bone ossification in humerus, radius and ulna. Hindlimb bones tibia and fibula were shortened or bent, respectively, with the femur being less affected. (A) *n*=10 each; (B) *n*=20 for WT, *n*=19 for cko. cl, clavicle; cs, coronal suture; f, frontal; fe, femur; fi, fibula; h, humerus; ip, intraparietal; ma, mandible; n, nasal; o.t., os tympanicum; p, parietal; pm, premaxilla; r, radius; s, scapula; t, tibia; u, ulna. Scale bars: 2 mm. See also Fig. S3.

(metacarpal/metatarsal number 6-7) with lack of the first digit, bifurcated middle metacarpals/metatarsals and bifurcated/trifurcated phalanges (Fig. 3D). Other mutants with increased Shh signaling such as *Prx1-Cre*; *Sufu*$^{f/-}$ and *Prx1-Cre*; *Ptch1*$^{f/f}$ also show increased digit fields (Zhulyn et al., 2014; Butterfield et al., 2009), although the later manifestations were not characterized due to late gestational lethality. Thus, increased Shh signaling in *Gpr161* cko results in polysyndactylous phenotypes.

Gpr161 determines endochondral and intramembranous bone formation

During later embryonic development in *Gpr161* cko mutants, the limb long bones were severely shortened (Fig. 4A,B). As apparent from skeletal staining with Alizarin Red (stains mineralized cartilage/bone) and Alcian Blue (stains unmineralized cartilage), there was no mineralization in the forelimb long bones, even at the end of gestation (Fig. 4A,B, Fig. S3B) or shortly after birth, beyond which point the embryos did not survive. However, mineralization in the digits in the *Gpr161* cko forelimbs was unaffected (Fig. 4B). The hindlimb long bones, in particular tibia and fibula, were shortened or bent, respectively, with the femur being relatively less affected (Fig. 4B). The relative strength of phenotypes in forelimb long bones with respect to hindlimb long bones is probably reflective of earlier and nearly complete deletion of *Gpr161* in forelimbs with respect to hindlimbs, based on earlier *Prx1-Cre* expression in forelimbs (Logan et al., 2002) (Fig. S3A). In addition, fusion of ribs and sternum in the ventral midline in *Gpr161* cko was absent (Fig. 4A, Fig. S3C). Thus, *Gpr161* cko forearm endochondral bones lacked mineralization.

In contrast to endochondral bone formation, intramembranous bones arise directly by mesenchymal differentiation compacted into sheets, and does not require a cartilage mold (Kronenberg, 2003; Abzhanov et al., 2007). Cranial vault (calvarium) and facial bones arise directly from deep layers of the dermis via intramembranous ossification (Abzhanov et al., 2007). In the mouse, the calvarial bones posterior to the coronal suture (posterior skull), except a part of the interparietal bones, are derived from cranial mesoderm, whereas frontal bone and facial bones are derived from the cranial neural crest cells (Chai and Maxson, 2006). Interestingly, coincident with *Prx1-Cre* expression in cranial mesenchyme (Fig. S3A) (Logan et al., 2002; Goodnough et al., 2012), there was a complete lack of posterior skull mineralization in *Gpr161* cko (Fig. 4A). However, most of the frontal, facial bones and mesoderm-derived endochondral bones in the base of the skull, such as basioccipital and basisphenoid, were not affected (Fig. 4A, Fig. S3D). Most of the scapula also ossifies by intramembranous ossification, and in *Gpr161* cko scapular ossification was mostly lacking (Fig. 4B). Thus, *Gpr161* cko are lacking in intramembranous bone formation.

Sustained proliferation of periarticular/round chondrocytes during endochondral bone formation in *Gpr161* conditional knockout

We further investigated the reasons for the lack of mineralization in the forelimb long bones in *Gpr161* cko. We detected a complete lack of trabecular long bone and bone collar formation in forelimb long bones using von Kossa staining, and noticed concomitant accumulation of cartilage using Safranin O staining at E17.5

Development (2018) 145, dev154054. doi:10.1242/dev.154054

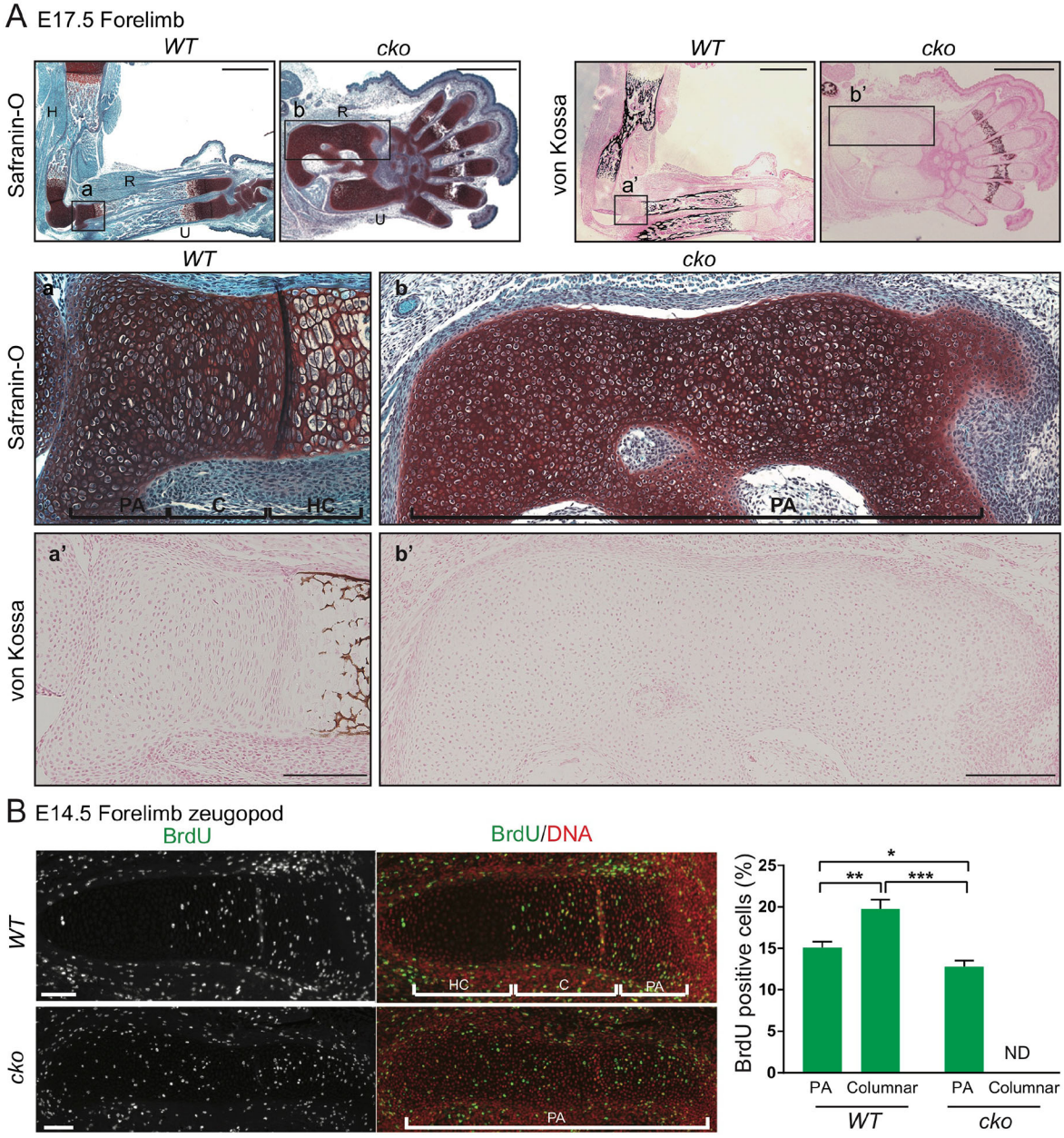

Fig. 5. Lack of maturation and sustained proliferation of periarticular/round chondrocytes in *Gpr161* cko. (A) Serial sections from E17.5 *Prx1-Cre; Gpr161*$^{fl/+}$ (WT) (*n*=2) and *Prx1-Cre; Gpr161*$^{fl/f}$ (cko) (*n*=4) forelimbs were stained by Safranin O and von Kossa. Magnified regions of the boxed regions are shown in the panels beneath. Note complete lack of von Kossa staining in *Gpr161* cko, with chondrogenesis throughout the areas of the long bones. Magnification of the radius (b) shows a complete lack of columnar and hypertrophic chondrocytes. Only a few columnar and hypertrophic chondrocytes are visible in magnification of the proximal ulna (shown in Fig. S4A). Perichondrium in *Gpr161* cko also lacks von Kossa staining. (B) E14.5 *Prx1-Cre; Gpr161*$^{fl/+}$ (WT; *n*=3), *Prx1-Cre; Gpr161*$^{fl/f}$ (cko; *n*=5) forelimbs sectioned horizontally were immunostained for BrdU (green; 3 h pre-labeled), and counter-stained for DNA (red). For WT the distal radius is shown. For cko, the whole forearm long bone is shown. Proximal side of the bone is to the left for both WT and cko. Note continued proliferation of chondrocytes throughout the extent of the forelimb long bone in *Gpr161* cko. BrdU incorporation was measured in periarticular/round and columnar chondrocytes in WT, and periarticular/round-like chondrocytes in *Gpr161* cko. ND, not determined (columnar chondrocytes were almost completely absent in *Gpr161* cko). Data were acquired from a total of seven or eight individual regions from two separate embryos of each genotype. Data represent mean±s.e.m. **P*<0.05, ***P*<0.01, ****P*<0.001 by one-way ANOVA with Tukey's post-hoc multiple comparison tests. C, columnar; H, humerus; HC, hypertrophic chondrocytes; PA, periarticular/round; R, radius; U, ulna. Scale bars: 1 mm (A, top panels); 200 µm (A, middle and bottom panels); 100 µm (B). See also Fig. S4.

(Fig. 5A). During endochondral bone formation, the periarticular/round chondrocytes mature into columnar chondrocytes, which further differentiate into prehypertrophic and hypertrophic chondrocytes (Kronenberg, 2003). In *Gpr161* cko embryos, we noted that round chondrocytes were predominantly present throughout the forelimb long bones, and there was an almost complete lack of columnar and hypertrophic chondrocytes at E17.5 (Fig. 5A, Fig. S4A). To confirm further the steps where chondrocyte maturation is blocked, we quantified proliferation by measuring incorporation after an acute pulse of bromodeoxyuridine (BrdU). BrdU incorporation in periarticular/round chondrocytes has been shown to be lower than that in columnar chondrocytes, with no

Development (2018) 145, dev154054. doi:10.1242/dev.154054

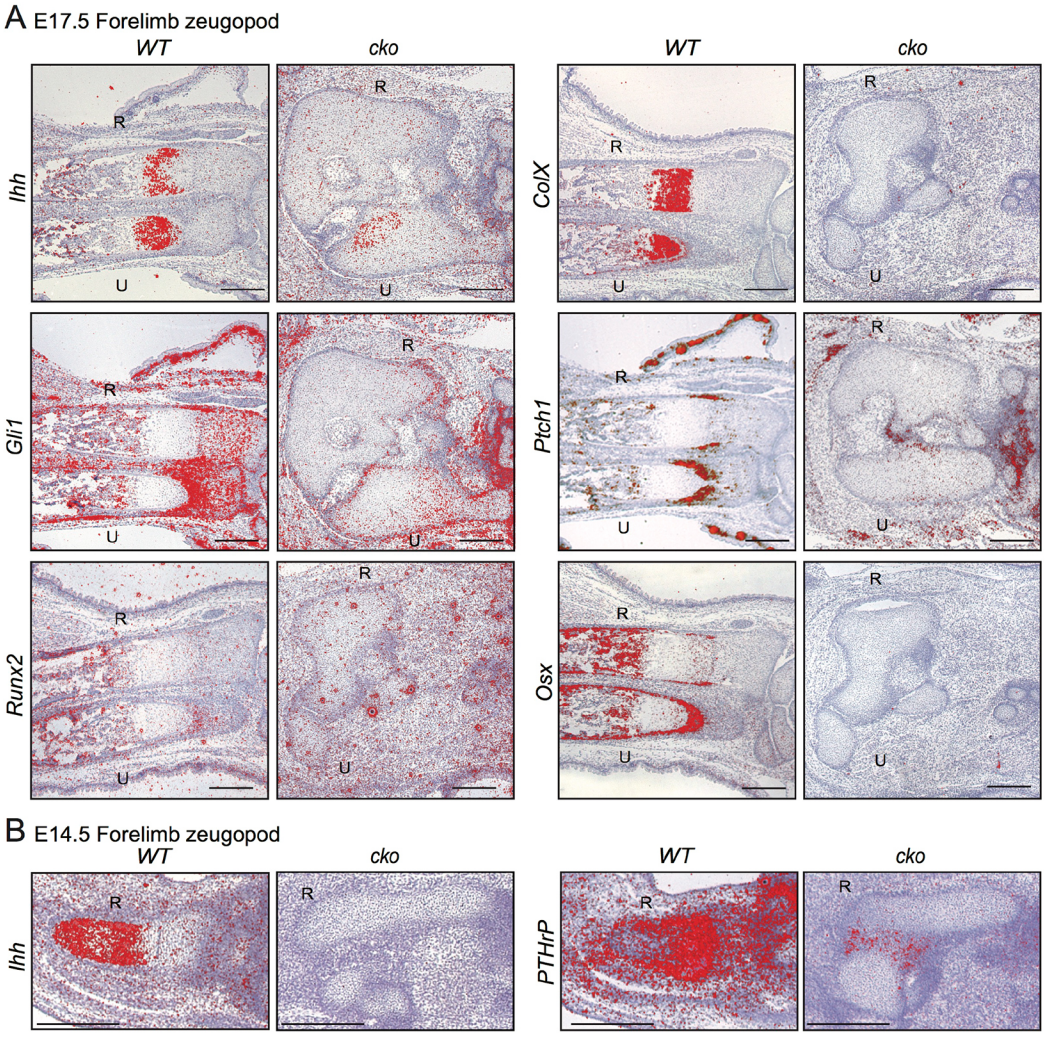

Fig. 6. Decreased Ihh signaling in *Gpr161* cko. (A) E17.5 *Prx1-Cre; Gpr161*$^{fl/+}$ (WT) (*n*=1) and *Prx1-Cre; Gpr161*$^{f/f}$ (cko) (*n*=2) forelimbs sectioned horizontally were probed for expression of designated transcripts using radioisotopic *in situ* hybridization (pseudocolored red), and counterstained with Hematoxylin. For WT, the distal radius and ulna are shown. For cko, the whole forearm long bones are shown. Distal side of the bone is to the right. The transcripts probed were Ihh targets *Ptch1* and *Gli1* (perichondrium and proliferating chondrocytes), *Ihh* (prehypertrophic and hypertrophic chondrocytes), *Col X* (hypertrophic chondrocytes), *Runx2* (osteoblast progenitors) and *Osx* (immature osteoblasts). Note lack of *Ihh* and Ihh target expression, lack of *ColX* (secreted by hypertrophic chondrocytes), and osteoblast progenitors in long bones of the forearm of *Gpr161* cko. Note that adjacent autopods exhibit *Ihh* and Ihh target expression, and that skin hair follicles exhibit Shh pathway activation (*Ptch1*, *Gli1* expression) as shown in Fig. S5B. (B) E14.5 *Prx1-Cre; Gpr161*$^{fl/+}$ (WT) (*n*=2 sides) and *Prx1-Cre; Gpr161*$^{f/f}$ (cko) (*n*=8 sides) embryos sectioned horizontally at forelimb levels were probed for expression of *Ihh* and *PTHrP* (periarticular cartilage). For WT, the distal radius and ulna are shown. For cko, the whole forearm long bones are shown. Distal side of the bone is to the right. Note lack of *Ihh* and reduced *PTHrP* transcripts in *Gpr161* cko. See complete horizontal sections depicting both the forearms, along with the regions shown in B in Fig. S5C. R, radius; U, ulna. Scale bars: 500 µm.

BrdU incorporation in the differentiating hypertrophic chondrocytes (Kobayashi et al., 2005, 2002). In the *Gpr161* cko, BrdU-positive round chondrocytes persisted throughout the forelimb long bones (Fig. 5B), lacked the typical anatomy of columnar chondrocytes (Fig. 5A), and had BrdU incorporation rates lower than columnar chondrocytes from littermate controls (Fig. 5B). Cyclin D1 and p130 (*Rbl2*), one of the Rb proteins, are expressed complementary to each other in proliferating and hypertrophic chondrocytes, respectively (Fig. S4B) (Yang et al., 2003; Long et al., 2001). In line with the persistence of proliferating chondrocytes throughout the forearm long bones in *Gpr161* cko, cyclin D1 was present in these chondrocytes, along with an absence of p130 (Fig. S4B). Compared with forearms, ossification in hindlimb long bones was less affected or not affected, with lack of von Kossa staining only in tibia (Fig. S4C). Thus, lack of *Gpr161* prevents chondrocyte maturation beyond the periarticular/round chondrocyte stage.

Lack of Ihh signaling and osteoblast differentiation in *Gpr161* conditional knockout

We further tested the failure of maturation of chondrocytes, with respect to Ihh signaling, and osteoblast differentiation in the *Gpr161* cko using radioisotopic *in situ* hybridization for detecting expression of relevant transcripts. Columnar chondrocytes differentiate into prehypertrophic and hypertrophic chondrocytes that express and secrete *Ihh* and collagen X (*ColX*; *Col10*). Ihh increases *Gli1* and *Ptch1* levels in proliferating chondrocytes and in adjacent perichondrium. Ihh also results in production of parathyroid hormone-like peptide (PTHrP) in periarticular cartilage, which prevents differentiation of columnar to prehypertrophic chondrocytes in a negative-feedback loop (Lanske et al., 1996; Vortkamp et al., 1996) (Fig. S5A).

Coincident with a lack of pre-hypertrophic and hypertrophic chondrocytes, there was an almost-complete lack of *Ihh* and *ColX*

Development (2018) 145, dev154054. doi:10.1242/dev.154054

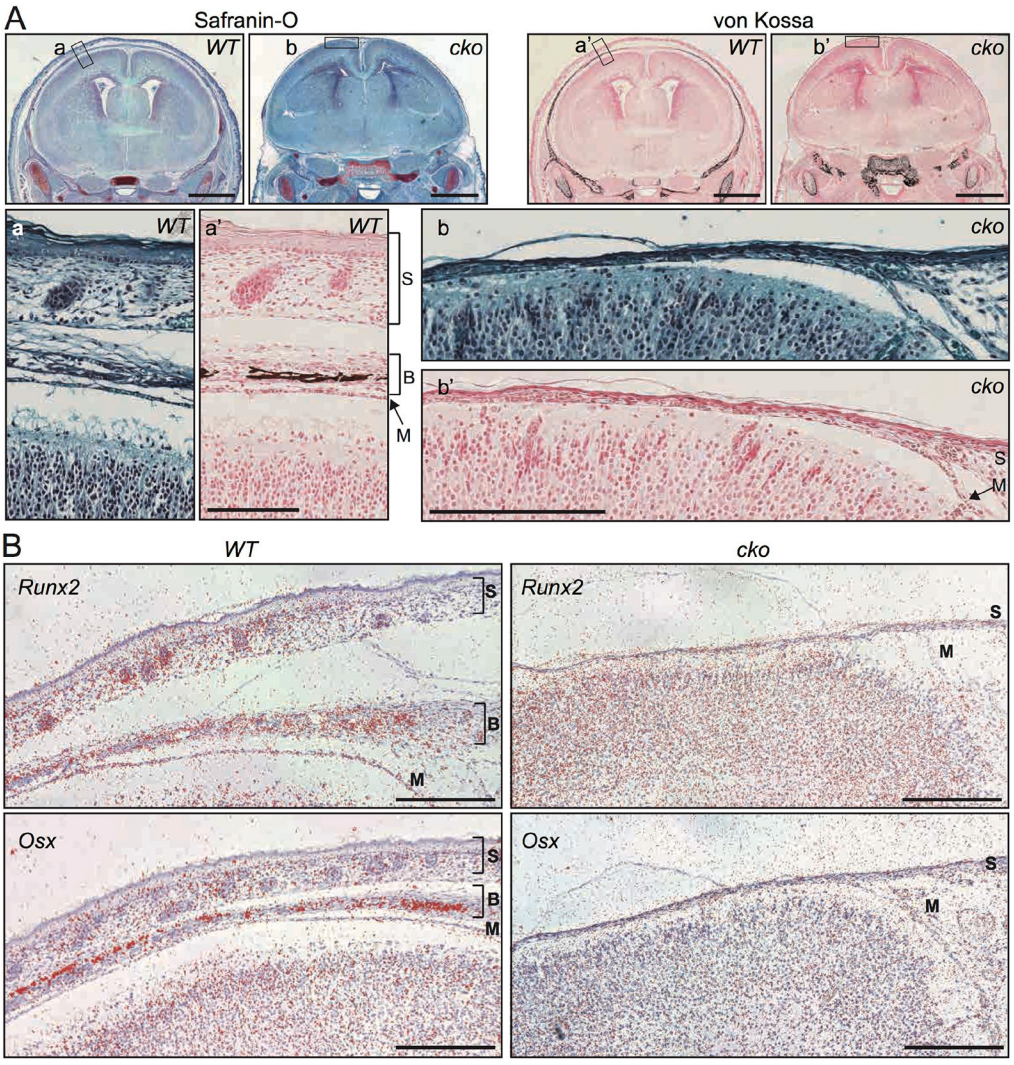

Fig. 7. Lack of intramembranous ossification and osteoblast differentiation in *Gpr161* cko. (A) E17.5 *Prx1-Cre; Gpr161*$^{fl/+}$ (WT) and *Prx1-Cre; Gpr161*$^{fl/f}$ (cko) head sectioned coronally at the level of lateral ventricles were stained with Safranin O (left) and von Kossa (right). Note that *Gpr161* cko shows lack of calvarium ossification with persistence of ossification and chondrogenesis at the base of the skull. Magnifications of the boxed areas shown below demonstrate lack of calvarium ossification or compensatory chondrogenesis in *Gpr161* cko. The skin overlying the missing cranium was also dramatically thinner in *Gpr161* cko. *n*=3 sections each. (B) E17.5 *Prx1-Cre; Gpr161*$^{fl/+}$ (WT) and *Prx1-Cre; Gpr161*$^{fl/f}$ (cko) embryo heads sectioned coronally were probed for expression of *Runx2*, and *Osx* by radioisotopic *in situ* hybridization as in Fig. 4. Medial regions are shown. Note lack of *Runx2* and *Osx* in calvarium of *Gpr161* cko with respect to WT. *Runx2* is also expressed in developing dermal papillae in WT (Glotzer et al., 2008). *n*=3 sections each. B, bone; M, meninges; S, skin. Scale bars: 1 mm (A, top panels); 200 µm (A, lower panels; B).

transcripts at E17.5 in the forearm long bones in *Gpr161* cko versus littermate controls (Fig. 6A). Both *Gli1* and *Ptch1* transcripts were reduced in the proliferating chondrocytes and perichondrium at E17.5, consistent with lack of Ihh signaling (Fig. 6A). In addition, *Ihh* expression was lacking at E14.5, and expression of *PTHrP* (*Pthlh*) transcripts was also reduced (Fig. 6B, Fig. S5C). We further tested expression of the osteoblast progenitor marker *Runx2* and the early osteoblast marker *Osx* (*Sp7*) in the trabecular bone and bone collar. Both transcripts were completely absent in the forearm long bones in *Gpr161* cko (Fig. 6A). Interestingly, the forelimb autopods showed retention of mineralization and bone ossification (Fig. 4B, Fig. 5A), chondrocyte maturation, Ihh signaling, and osteoblastogenesis (Fig. S5B), despite similar knockdown of *Gpr161* transcripts compared with the forearm, reflecting regional specificity in bone ossification programs in the forelimb. As seen with mineralization and bone ossification (Fig. 4B, Fig. S4C), the hindlimb long bones were less affected or not affected with respect to expression of *Ihh*, Ihh target genes, and osteoblast maturation (Fig. S5D). Thus, forearm long bones in *Gpr161* cko show lack of Ihh signaling, along with an absence of Ihh-secreting hypertrophic chondrocytes. Simultaneously, there is a complete lack of osteoblastogenesis in trabecular bone and bone collar.

Intramembranous ossification defects and lack of compensatory chondrogenesis in *Gpr161* conditional knockout

We confirmed the complete lack of ossification in the posterior calvarium by von Kossa staining in E17.5 *Gpr161* cko embryos, but noted no compensatory accumulation of cartilage using Safranin O (Fig. 7A). In addition, using *in situ* hybridization we determined that *Runx2* and *Osx* transcripts were completely missing in the calvarium of *Gpr161* cko embryos, corresponding to the lack of ossification (Fig. 7B). Similar to the *Runx2* knockout (Komori et al., 1997), which also lack intramembranous bone formation in calvarium, there was barely any other layer of cells between the skin and meninges. The skin layers, including the dermis overlying the missing cranium, were also dramatically thinner (Fig. 7A,B). Thus, osteoblastogenesis is completely blocked during intramembranous bone morphogenesis with no compensatory chondrogenesis in *Gpr161* conditional mutants.

Gpr161 determines limb patterning and skeletogenesis in a cilia-dependent manner

As Gpr161 localizes to the primary cilia, we tested the role of cilia in phenotypes resulting from *Gpr161* deletion by combining with deficiencies in the IFT-B complex protein *Ift88* that disrupt cilia. Conditional knockout of *Ift88* results in a smaller growth plate

Development (2018) 145, dev154054. doi:10.1242/dev.154054

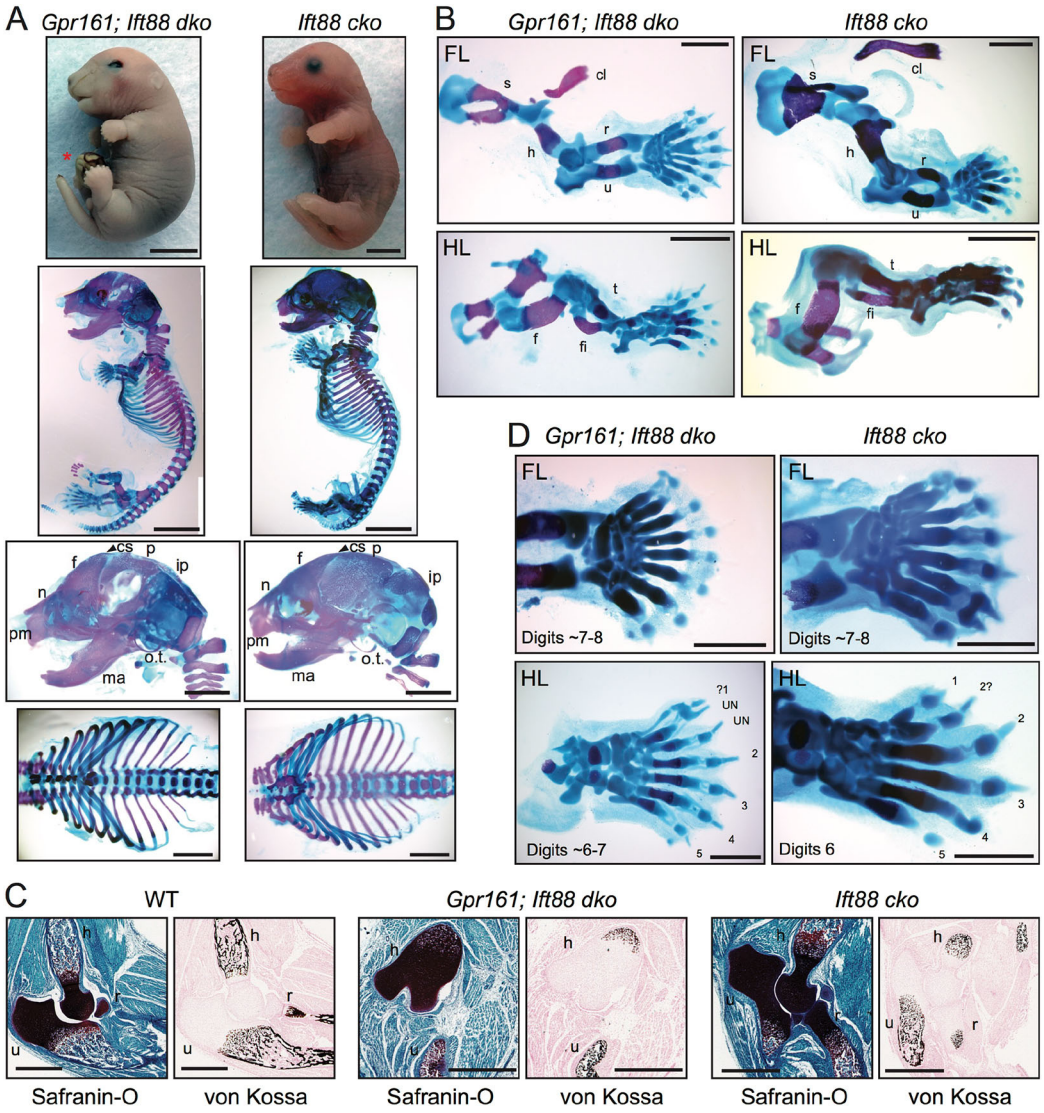

Fig. 8. Gpr161 determines limb patterning and skeletogenesis in a cilia-dependent manner. (A,B) Skeletal staining of *Prx1-Cre; Gpr161*$^{f/f}$*; Ift88*$^{f/f}$ (*Gpr161; Ift88* dko) and *Prx1-Cre; Ift88*$^{f/f}$ (*Ift88* cko) embryos as represented in Fig. 4. Red asterisk denotes cranial and anterior thoracic/abdominal wall defects. The posterior calvarium and most of the scapula were lacking in mineralization in *Gpr161* cko (Fig. 4), both of which were partially rescued in *Gpr161; Ift88* dko. The ribcage was lacking in sternum and the ventral ribs were not fused and were widely open in *Gpr161* cko, which were rescued in *Gpr161; Ift88* dko. The lack of mineralization in forearm long bones in *Gpr161* cko was also rescued in *Gpr161; Ift88* dko. (A) *n*=5 each; (B) *n*=6 for *Gpr161; Ift88* dko and *n*=9 for *Ift88* cko. (C) Serial sections from postnatal day 0 *Prx1-Cre; Gpr161*$^{f/+}$ (WT), *Gpr161; Ift88* dko, and *Ift88* cko forelimbs were stained by Safranin O and von Kossa. Unlike *Gpr161 cko* (Fig. 5A), endochondral bone formation in forelimb long bones was restored as seen using von Kossa staining in the *Gpr161; Ift88* dko. *n*=3 sections each. (D) Alcian Blue and Alizarin staining of forelimb autopods and feet in E18.5 *Gpr161; Ift88* dko (*n*=6) and *Ift88* cko (*n*=9). Digits in *Ift88* cko and *Gpr161; Ift88* dko autopods look identical with lack of syndactyly and extra phalanges, as seen in the *Gpr161* cko (Fig. 3). The *Ift88* cko feet show preaxial polydactyly, and *Gpr161; Ift88* dko feet are similar to *Ift88* cko with a rudimentary digit 1, extra second digit, and completely lacking bifurcated metatarsals or extra phalanges. cl, clavicle; cs, coronal suture; f, frontal; fi, fibula; h, humerus; ip, intraparietal; ma, mandible; n, nasal; o.t., os tympanicum; p, parietal; pm, premaxilla; r, radius; s, scapula; t, tibia; u, ulna; UN, unassigned digits. Scale bars: 2 mm (A,B); 1 mm (C,D). See also Fig. S6.

during endochondral bone formation, without affecting ossification and intramembranous bone formation (Haycraft et al., 2007; Song et al., 2007). We generated single conditional knockouts of *Prx1-Cre*; *Ift88*$^{f/f}$ (*Ift88* cko) and double conditional knockouts of *Prx1-Cre*; *Ift88*$^{f/f}$; *Gpr161*$^{f/f}$ (*Gpr161*; *Ift88* dko) (Fig. 8A). Primary cilia were completely missing in chondrocytes and surrounding perichondrium in *Ift88* cko and *Gpr161*; *Ift88* dko, unlike littermate controls, which were ciliated (Fig. S6A).

Strikingly, *Ift88* was genetically epistatic to *Gpr161* in skeletal morphogenesis and limb patterning as described below. First, the endochondral and intramembranous bone mineralization phenotypes in *Gpr161* cko are cilia dependent. *Gpr161* cko showed lack of mineralization of forelimb long bones, absent posterior skull, lack of sternum and no rib fusion (Fig. 4). Remarkably, the *Gpr161; Ift88* dko rescued mineralization in the forearm long bones, and rib fusion in the ventral midline (Fig. 8A, B). Unlike *Gpr161* cko, which lack ossification, we detected restoration of endochondral bone formation in forelimb long bones using von Kossa staining (Fig. 8C), and concomitant generation of columnar and hypertrophic chondrocytes using Safranin O staining in the *Gpr161*; *Ift88* dko (Fig. 8C, Fig. S6A). Thus, concomitant *Ift88* deficiency prevents endochondral ossification

Development (2018) 145, dev154054. doi:10.1242/dev.154054

phenotypes arising in the *Gpr161* cko. Interestingly, the proliferating chondrocytes in *Gpr161* cko were ciliated, irrespective of BrdU labeling and cyclin D1 expression (Fig. S6B,C). Therefore, chondrocyte proliferation in *Gpr161* cko might undergo a cilia-dependent pathway. Second, intramembranous bone formation in cranium and scapula was partially restored in *Gpr161*; *Ift88* dko. Particularly, frontal bones and most of the parietal bones were formed, with regions in the posterolateral parietal bones still lacking mineralization, but with no compensatory chondrogenesis (Fig. 8A,B). Thus, concomitant *Ift88* deficiency prevents intramembranous ossification defects arising in the *Gpr161* cko. Third, lack of cilia in *Gpr161*; *Ift88* dko embryos prevented syndactyly, bifurcated metacarpals/metatarsals and bifurcated/trifurcated phalanges (Fig. 8C), as observed in *Gpr161* cko autopods (Fig. 3D). Instead, *Gpr161*; *Ift88* dko autopods had phenotypes resembling *Ift88* cko, such as preaxial polydactyly in feet (Fig. 8C) (Haycraft et al., 2007). Thus, patterning defects in *Gpr161* cko limbs are cilia dependent.

DISCUSSION

Limb and skeletal morphogenesis phenotypes in *Gpr161* mutants

The importance of basal suppression of Shh pathway, its interaction with Ihh signaling, and the role of cilia-dependent signaling during limb and skeletal morphogenesis is not well understood. Here, using detailed phenotypic analysis of germline and conditional *Gpr161* knockouts, we uncover multiple crucial steps that are regulated by Gpr161. First, we show that forelimbs are not formed in *Gpr161* knockouts, despite establishment of *Tbx5*-expressing prospective limb fields. Second, we show that limb-specific deletion of *Gpr161* caused premature expansion of Shh signaling resulting from lack of Gli3R activity. *Gpr161* deletion also caused ectopic Shh expression and increased pathway activity. Defective limb bud patterning from increased Shh signaling caused polysyndactyly affecting middle digits. Third, we demonstrate that endochondral bone formation (both bone collar and trabecular bone) in forearm was severely affected upon limb-specific *Gpr161* deletion. Proliferating round/periarticular-like chondrocytes failed to differentiate into columnar chondrocytes and accumulated in forearms, along with a corresponding absence of Ihh signaling. Thus, Gpr161 inhibits periarticular chondrocyte proliferation. Fourth, we show that ossification in posterior skull and scapula were disrupted in *Gpr161* conditional knockouts, suggesting that Gpr161 promotes osteoblastogenesis during intramembranous bone formation. Finally, we demonstrate that defects in limb patterning, endochondral and intramembranous skeletal morphogenesis were suppressed in the absence of cilia, indicating that the pathways affected upon Gpr161 deletion are cilia-dependent (Fig. 9).

The role of Gpr161 in forelimb bud formation

Limb bud formation is orchestrated through the following stages (Duboc and Logan, 2011): (1) an induction stage during which axial cues and a combinatorial Hox code confers limb-forming potential to the lateral plate mesoderm; (2) an initiation stage during which *Tbx5* or *Tbx4* are expressed in the presumptive forelimb- or hindlimb-forming areas, respectively, followed by *Fgf10*; and (3) an outgrowth stage when a stable positive-feedback loop between mesenchymal *Fgf10* and ectodermal *Fgf8* is established. *Prx1-Cre; Tbx5*$^{f/f}$ has been shown to lack forelimbs (Rallis et al., 2003), whereas Fgf10 is required for both forelimb and hindlimb development (Sekine et al., 1999; Ohuchi et al., 1997). Although *Fgf10* has been proposed to be a direct transcriptional target of Tbx5 (Agarwal et al., 2003; Ng et al., 2002), other inputs, including retinoic acid, also regulate *Fgf10* expression (Nishimoto et al., 2015).

The specificity of *Gpr161* knockouts in preventing formation of forelimbs, but not of hindlimbs, rules out indirect effects affecting forelimb formation. As *Tbx5* is expressed in the prospective forelimb field in *Gpr161* knockouts, unlike *Fgf10*, Gpr161 is likely to function in forelimb initiation or outgrowth at a step that facilitates the function of Tbx5, upstream of *Fgf10*. The most parsimonious model would be that Gpr161 functions by promoting Gli3R generation and preventing premature Shh signaling in the prospective forelimb field (Fig. 9A). Alternatively, Gpr161 might be affecting other cellular pathways in preventing forelimb bud formation (Feigin et al., 2014).

The role of restricting premature Shh signaling in the prospective forelimb field during forelimb initiation has not been formally tested. First, premature activation of Shh pathway by deleting *Ptch1* using *Prx1-Cre*, which expresses after *Tbx5* (Nishimoto et al., 2015; Minguillon et al., 2012), results only in forelimb outgrowth defects stemming from a lack of Gli3R-dependent specification of anterior progenitors (Butterfield et al., 2009; Zhulyn et al., 2014). Second, knockouts of other negative regulators of the Shh pathway, such as *Ptch1* and *Sufu*, arrest by E9-9.5 (Goodrich et al., 1997; Svärd et al., 2006). The embryonic lethality of *Gpr161* knockouts at E10.5, at an age after limb buds are established, allows a window of opportunity for looking into the role of suppression of premature Shh signaling in forelimb bud formation. However, unlike *Gpr161* knockouts, *Gli3* knockout mice possess forelimbs (Litingtung et al., 2002). Thus, a combination of a lack of Gli3R formation and increased GliA generation might be necessary for preventing forelimb formation (Fig. 9A).

The role of Gpr161 in chondrocyte proliferation

Gpr161 cko forearm long bones were composed of proliferating chondrocytes similar to periarticular/round chondrocytes, as determined by BrdU incorporation and morphology. This could result from a direct role of Gpr161 in preventing periarticular/round chondrocyte proliferation. Alternatively, lack of Ihh formation in *Gpr161* cko could prevent differentiation into columnar chondrocytes (Kobayashi et al., 2002, 2005). Gli3, particularly the Gli3R form, has been proposed to function as a repressor of Ihh-mediated differentiation of periarticular into columnar chondrocytes, rather than in earlier chondrocyte proliferation (Koziel et al., 2005). Of note, *Gli3*; *Ihh* double knockouts rescue the lack of columnar chondrocyte formation in *Ihh* knockouts (Koziel et al., 2005). Gpr161 loss prevents both Gli3R and Ihh formation, but the phenotype in *Gpr161* cko is unlike that of *Gli3*; *Ihh* double knockouts. Thus, Gpr161 functions as a rheostat in preventing proliferation of periarticular chondrocytes, upstream of Ihh-mediated and Gli3R-suppressed differentiation of periarticular to columnar chondrocytes (Fig. 9C).

The role of Gpr161 in endochondral osteoblastogenesis

Gpr161 cko forearm long bones showed a complete lack of *Runx2*-expressing osteoblast progenitors and osteoblastogenesis. Ihh determines osteoblast differentiation during bone collar formation in endochondral bone (St-Jacques et al., 1999; Long et al., 2004). However, absence of bone collar formation is more severe in *Gpr161* cko forelimbs compared with *Ihh* knockouts or conditional/mosaic knockouts of *Smo*, the activator of the hedgehog pathway (Long et al., 2004). The persistence of periarticular/round chondrocyte proliferation along with lack of Ihh signaling might

Development (2018) 145, dev154054. doi:10.1242/dev.154054

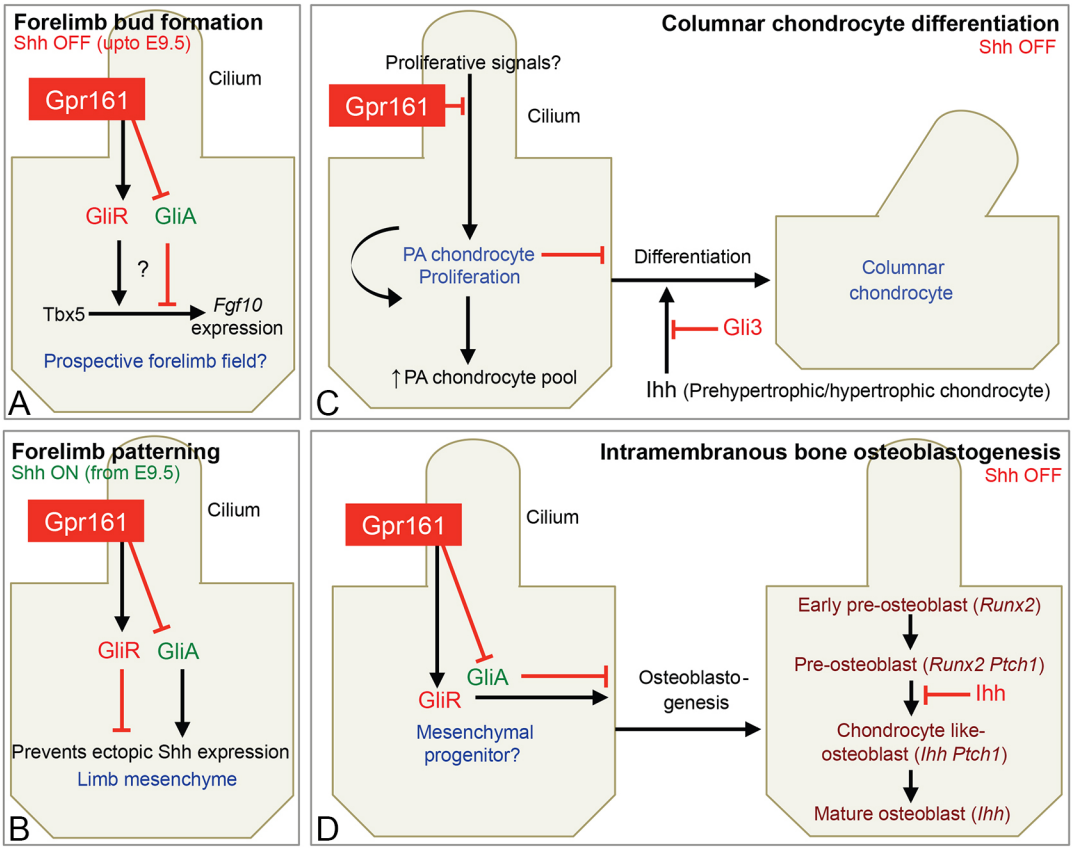

Fig. 9. Role of Gpr161 in forelimb initiation, limb patterning and skeletal morphogenesis. (A) Gpr161 determines Gli3R formation prior to Shh expression preventing premature signaling. Premature activation of the Shh pathway might prevent forelimb bud formation by regulating *Fgf10* expression downstream of Tbx5. (B) Gpr161 prevents ectopic Shh expression and Shh-regulated limb patterning in a cilia-dependent manner. (C) In the absence of Gpr161, continued slow proliferation of periarticular/round (PA) chondrocytes is mediated by cilia-regulated pathway/s. Proliferative signals and mechanisms underlying Gpr161-mediated inhibition of proliferation are currently unknown. (D) During intramembranous bone formation, Gpr161 blocks a cilia-generated signaling pathway inhibiting osteoblastogenesis, possibly by functioning in calvarial mesenchymal progenitors that precede *Runx2* expressing pre-osteoblasts. The cilia-generated pathway could be premature Ihh/Shh signaling. Stages of osteoblast differentiation are based on previous literature (Abzhanov et al., 2007).

explain the severity of lack of bone ossification in the *Gpr161* cko. Less severe bone collar defects in *Col2a1-cre; Ptch1*$^{f/f}$ mutants (Mak et al., 2006) with respect to *Gpr161* cko mutants could result from inefficient knockout in perichondrium or developing periosteum in the former.

The role of Gpr161 in intramembranous osteoblastogenesis

Lack of skull ossification in *Gpr161* cko is similar to that observed in *Runx2* and *Osx* knockouts (Otto et al., 1997; Komori et al., 1997; Nakashima et al., 2002) and *Prx1-Cre; Runx2* conditional knockouts (Takarada et al., 2016). In *Gpr161* cko, *Runx2* and *Osx* expression in the presumptive calvarium was inhibited. Therefore, the promotion of osteoblastogenesis by Gpr161 might initiate in calvarial mesenchymal progenitors that precede the appearance of *Runx2*-expressing pre-osteoblasts (Abzhanov et al., 2007). The skin layers, including the dermis overlying the missing cranium, were also dramatically thinner in *Gpr161* cko. Wnt ligands released from the epidermis regulate both dermis condensation and cranial intramembranous bone specification (Goodnough et al., 2012; Chen et al., 2012). Mutants with conditional deletion of β-catenin lack intramembranous bone, but have compensatory chondrogenesis (Hill et al., 2005; Day et al., 2005; Tran et al., 2010). Rather, the simultaneous lack of intramembranous bone morphogenesis and compensatory cartilage formation in posterior skull in *Gpr161* cko is similar to overactivation of β-catenin in cranial mesenchyme (Goodnough et al., 2012). Future work should focus on understanding the link between Gpr161 and β-catenin signaling in regulating intramembranous bone formation, compensatory chondrogenesis, and cranial dermis development.

The role of cilia-dependent signaling in skeletal morphogenesis

The sustained proliferation and accumulation of periarticular/round chondrocytes seen in *Gpr161* cko was suppressed in the absence of cilia, indicating that the chondrocyte proliferation step is likely to be cilia dependent. Hedgehog signaling targets such as *Gli1* and *Ptch1* were not upregulated in the periarticular chondrocytes. Periarticular chondrocytes possess cilia embedded in the ciliary pocket and are surrounded by the cartilaginous extracellular matrix, raising the possibility that certain unknown, possibly mechanosensory, stimuli might regulate chondrocyte proliferation (Malone et al., 2007; Xiao et al., 2006) (Fig. 9C).

The lack of intramembranous bone formation in *Gpr161* cko was suppressed in the absence of cilia. Thus, Gpr161 blocks a cilia-generated signaling pathway inhibiting osteoblastogenesis during intramembranous bone formation. Premature Ihh/Shh signaling could be the cilia-generated pathway that inhibits intramembranous

Development (2018) 145, dev154054. doi:10.1242/dev.154054

osteoblastogenesis (Fig. 9D). First, conditional knockouts of negative regulators of the Shh pathway, *Ptch1* (Mak et al., 2006), *Sufu* (Li et al., 2017) and *Gpr161*, show lack of skull formation. Deletion of *Sufu* in the cranial neural crest activates *Gli1* levels in cranial mesenchyme (Li et al., 2017). Second, simultaneous deletion of *Gli2* restores calvarial bone formation in the *Sufu* conditional knockouts (Li et al., 2017). Finally, *Ihh* and *Shh* are expressed in the osteogenic front of the developing intramembranous bone (Kim et al., 1998; Lenton et al., 2011), and, by direct binding to *Ptch1* expressed in pre-osteoblasts and chondrocyte-like osteoblasts, prevent further osteoblastogenesis (Abzhanov et al., 2007).

Overall, studying *Gpr161* mutant phenotypes provides the molecular, subcellular and cellular resolution required for understanding cilia-dependent processes in limb bud formation, chondrocyte proliferation and intramembranous osteoblastogenesis.

MATERIALS AND METHODS

Mouse strains

Targeting of the fourth exon of *Gpr161* (NM_001081126.1) by homologous recombination in mouse ESCs of the C57BL/6 strain was carried out by EUCOMM. The ESCs were injected into host embryos of the C57BL/6 albino strain by the transgenic core (Dr Robert Hammer's laboratory, UT Southwestern Medical Center, Dallas, TX, USA). The mutant germline allele was crossed with germline Flp-O (Jackson Laboratory, stock #012930) for deleting the FRT-LacZ-Neo-FRT cassette to generate the exon 4 floxed allele (Fig. S1A). This floxed line was crossed with *Prx1-Cre* (Logan et al., 2002; Jax strain #005584). The targeted recombination results in deletion of most of the fourth exon, except its initial 461 bp. This results in truncation of Gpr161 after its initial 153 amino acids (NP_001074595.1). Simultaneously, crossing with *CAG-Cre* recombinase line (Sakai and Miyazaki, 1997), in which *Cre* is expressed ubiquitously, generated the *Gpr161* knockout allele (Fig. S1A). Genotyping of *Gpr161* alleles was performed using primers in the deleted fourth exon (P1; 5′ CAAGATGGATTCGCAGTAGCTTGG), flanking the 3′ end of the deleted exon (P2; 5′ ATGGGGTACACCATTGGATACAGG), and in the Neo cassette (P3, 5′ CAACGGGTTCTTCTGTTAGTCC). Wild-type, floxed and knockout bands were 816, 965 and 485 bp, respectively (Fig. S1A). Double mutant analysis was performed using *Ift88* conditional allele (Haycraft et al., 2007; Jax strain #022409). Yolk sac DNAs were used for genotyping embryos. Noon of the day on which a vaginal plug was found was considered E0.5. All the animals in the study were handled according to protocols approved by the UT Southwestern Institutional Animal Care and Use Committee, and the mouse colonies were maintained in a barrier facility at UT Southwestern, in agreement with the State of Texas legal and ethical standards of animal care.

Antibodies and reagents

The affinity purified polyclonal antibody against Gpr161 was described previously (Pal et al., 2016) (1:200). Other commercial antibodies and reagents are described in supplementary Materials and Methods.

Primary cell culture, reverse transcription, quantitative PCR and immunoblotting

Primary cell culture, reverse transcription and quantitative PCR were performed according to standard protocols and are described in supplementary Materials and Methods. Embryos were processed for Gli1/3 immunoblotting as described previously (Wen et al., 2010).

In situ hybridization (ISH)

Antisense riboprobes were made using the following templates: *Ptch1*, *Gli1*, *Shh*, *Ihh* (from Andrew McMahon's lab, University of Southern California, CA, USA; and from Deanna Grant, Andrew Peterson's lab, Genentech, South San Francisco, CA, USA), *Tbx5* (from Virginia Papaioannou's lab, Columbia University, NY, USA), *Sox9*, *Col2a1* (from Steven Vokes lab, UT Austin), *Fgf10*, *Hoxd13* (from Xin Sun lab, University of Wisconsin, Madison) (Sun et al., 2002), *Osx*, *ColX* (from Rhonda Bassel-Duby, Eric Olson Lab, UT Southwestern Medical Center, Dallas), *Runx2* (from Yingzi Yang lab, Harvard School of Dental Medicine), and *PTHrP* (from Henry Kronenberg lab, Massachusetts General Hospital). Whole-mount *in situ* hybridization using digoxigenin-labeled probes was performed on embryos using standard protocols. Images were acquired using a Leica stereomicroscope (M165 C) with digital camera (DFC500) or Zeiss stereomicroscope (Discovery.V12) and AxioCam MRc.

Radiolabeled sense and antisense probes were generated by Sp6, T3 or T7 RNA polymerases and ^{35}S-UTP (>1000 Ci/mmol; NEG039H, PerkinElmer LAS Canada) using linearized cDNA templates by *in vitro* transcription using the Maxiscript kit (AM1324 M, Life Technologies). Radioisotopic *in situ* hybridization was performed as previously described (Shelton et al., 2000). Briefly, 5-µm-thick sections were deparaffinized, permeabilized and acetylated prior to hybridization at 70°C with riboprobes diluted in a mixture containing 50% formamide, 0.75 M NaCl, 20 mM Tris-HCl, pH 8.0, 5 mM EDTA, 10 mM $NaPO_4$, 14% dextran sulfate, 1× Denhardt's, and 0.5 mg/ml tRNA. Following hybridization, the sections were rinsed with increasing stringency washes, subjected to RNAse A (2 µg/ml, 30 min at 37°C) and dehydrated prior to dipping in K.5 nuclear emulsion gel (AGP9281; Ilford, UK). Autoradiographic exposure was conducted for 21 days to 35 days. Photographic development was carried out with D-19 Developer Substitute and Kodak Fixer (26920-4; 26942, Ted Pella). Sections were counterstained with Hematoxylin, dehydrated with ethanol, cleared with xylene, and cover slipped with synthetic mounting media (SP15, Fisher Chemical). Radioisotopic *in situ* hybridizations were analyzed using darkfield and brightfield microscopy. Sense (control) riboprobes established the level of background signal. Review and photography of all radioisotopic *in situ* hybridizations were carried out on a Leica DM2000 photomicroscope equipped with brightfield, and incident-angle darkfield illumination. Photomicrography was achieved using this microscope and an Optronics Microfire digital CCD color camera using PictureFrame 3.0 acquisition software (Optronics). The resulting ISH silver-grain signal was imaged with camera settings to produce near binary intensity and contrast. The ISH signal was pseudocolored red, and then overlaid to their concomitantly imaged brightfield image using Adobe Photoshop CS4 (Adobe Systems).

Skeletal staining

Skeletal preparations were made by a slight modification of the Alcian Blue/Alizarin Red staining procedure described by Kessel et al. (1990). Specimens were fixed in 99% ethanol for 24 h (embryos older than E15 were first de-skinned and eviscerated), and then kept in acetone for another 24 h. Incubation in staining solution (1 volume of 0.3% Alcian Blue in 70% ethanol, 1 volume of 0.1% Alizarin Red S in 96% ethanol, 1 volume of absolute acetic acid, and 17 volumes of 70% ethanol) was performed for 2-3 days at 37°C. Samples were rinsed in water and kept in 1% potassium hydroxide/20% glycerol at 37°C overnight, with additional incubation at room temperature until complete clearing. For long-term storage, specimens were transferred into 50%, 80% and finally 100% glycerol. Images were acquired using a Leica stereomicroscope (M165 C) with digital camera (DFC500).

Von Kossa and Safranin O staining

Von Kossa stain for calcification of mineralized cartilage/bone and Safranin O stain for cartilage were performed according to standard methods (Sheehan and Hrapchak, 1980; Bancroft and Stevens, 1990). In brief, von Kossa slides were deparaffinized, impregnated with 5% silver nitrate, developed with 5% sodium thiosulfate, and then counterstained with Nuclear Fast Red. Safranin O slides were deparaffinized, stained with Weigert's iron Hematoxylin, differentiated in acid-alcohol, counterstained with 0.2% Fast Green, de-stained with 1% acetic acid, and cartilaginous mucopolysaccharides colorized with 0.1% Safranin O before final differentiation with 95% ethanol. Following final differentiations and washes, von Kossa and Safranin O slides were dehydrated, cleared, and coverslipped with synthetic mounting media.

BrdU labeling and immunofluorescence and microscopy

Dams were injected intraperitoneally with 25 mg/kg BrdU and embryos collected 3 h post-injection. Embryos or limbs for histology were fixed in 20

Development (2018) 145, dev154054. doi:10.1242/dev.154054

volumes of freshly prepared 4% paraformaldehyde/PBS pH 7.4 (PFA). Harvested embryos were paraffin processed following PFA fixation. Following 2 N hydrochloric acid denaturation (BrdU) or pH 6.0 citra-based heat antigen-retrieval, serial sections were quenched of autofluorescence with 100 mM glycine and blocked against endogenous mouse IgG and secondary antibody host-serum affinity by utilizing commercially available blocking reagents (Vector Mouse on Mouse Kit, BMK-2202). Sections were incubated overnight at 4°C with primary antibody (anti-BrdU, 1:25 or other antibodies). For BrdU staining, subsequent biotin/streptavidin-fluorescein detection of bound primary was conducted the following day according to MOM kit instructions. Nuclei were counter stained with propidium iodide (5 µg/ml) prior to coverslipping with Vectashield (Vector Laboratories). Immunofluorescence of cultured cells and embryo cryosections was performed according to standard protocols after fixation in 4% PFA. The coverslips or cryosections were mounted using Fluoromount-G (Southern Biotech). Images were acquired on a Zeiss AxioImager.Z1 microscope, a PCO Edge sCMOS camera (BioVision Technologies), and PlanApochromat objectives (10×/0.45, 40×/1.3 oil, 63×/1.4 oil), controlled using Micromanager software at room temperature. Between 8 and 20 *z* sections at 0.5-0.8 µm intervals were acquired. Maximal projections from images of stacks were exported from ImageJ/Fiji using a custom written macro (Marcel Mettlen, Schmid lab, UT Southwestern Medical Center, and available upon request) using similar parameters (image intensity and contrast) for image files from the same experiment. Stereo images of embryos were taken on the Zeiss SteREO Discovery V.12 microscope using the 0.63× lens with AxioVision software and LEICA S8AP0 with LAS V4.8 software. Scanning electron microscopy was performed according to standard protocols and is described in supplementary Materials and Methods.

Statistical analyses

Statistical analyses were performed using Student's *t*-test for comparing two groups or Tukey's post-hoc multiple comparison tests between all possible pairs using GraphPad Prism.

Acknowledgements

We thank UT Southwestern's transgenic, molecular pathology, and electron microscopy cores for transgenic mouse generation, tissue processing and microscopy facilities. We thank the mouse animal care facility for animal care. We acknowledge gifts of reagents from Tamara Caspary, Andrew McMahon, Deanna Grant, Andrew Peterson, Virginia Papaioannou, Steven Vokes, Xin Sun, Rhonda Bassel-Duby, Eric Olson, Yingzi Yang and Henry Kronenberg. We thank Sandra Schmid, Issei Shimada, Fred Grinnell and anonymous reviewers for comments on the manuscript, and Jacek Topczewski and Peter Michaely for discussions.

Competing interests

The authors declare no competing or financial interests.

Author contributions

Conceptualization: S.H., J.A.R., S.M.; Methodology: S.H., K.A.W., B.N.S., J.M.S., S.M.; Formal analysis: S.H., K.A.W., B.N.S., J.M.S., J.A.R., S.M.; Investigation: S.H.; Resources: J.M.S.; Writing - original draft: S.M.; Writing - review & editing: S.H., K.A.W., B.N.S., J.M.S., J.A.R., S.M.; Visualization: S.M.; Supervision: S.M.; Project administration: S.M.; Funding acquisition: S.M.

Funding

This project was funded by a recruitment grant from the Cancer Prevention and Research Institute of Texas (R1220 to S.M.), a grant from the National Institutes of Health (1R01GM113023-01 to S.M.), and a Welch Foundation grant (I-1906 to S.M.). Deposited in PMC for release after 12 months.

Supplementary information

Supplementary information available online at
http://dev.biologists.org/lookup/doi/10.1242/dev.154054.supplemental

References

Abzhanov, A., Rodda, S. J., Mcmahon, A. P. and Tabin, C. J. (2007). Regulation of skeletogenic differentiation in cranial dermal bone. *Development* **134**, 3133-3144.

Agarwal, P., Wylie, J. N., Galceran, J., Arkhitko, O., Li, C., Deng, C., Grosschedl, R. and Bruneau, B. G. (2003). Tbx5 is essential for forelimb bud initiation following patterning of the limb field in the mouse embryo. *Development* **130**, 623-633.

Badgandi, H. B., Hwang, S.-H., Shimada, I. S., Loriot, E. and Mukhopadhyay, S. (2017). Tubby family proteins are adapters for ciliary trafficking of integral membrane proteins. *J. Cell Biol.* **216**, 743-760.

Bancroft, J. D. and Stevens, A. (1990). *Theory and Practice of Histological Techniques*. Edinburgh, New York: Churchill Livingstone.

Bitgood, M. J. and Mcmahon, A. P. (1995). Hedgehog and Bmp genes are coexpressed at many diverse sites of cell-cell interaction in the mouse embryo. *Dev. Biol.* **172**, 126-138.

Butterfield, N. C., Metzis, V., Mcglinn, E., Bruce, S. J., Wainwright, B. J. and Wicking, C. (2009). Patched 1 is a crucial determinant of asymmetry and digit number in the vertebrate limb. *Development* **136**, 3515-3524.

Chai, Y. and Maxson, R. E.Jr (2006). Recent advances in craniofacial morphogenesis. *Dev. Dyn.* **235**, 2353-2375.

Chen, D., Jarrell, A., Guo, C., Lang, R. and Atit, R. (2012). Dermal beta-catenin activity in response to epidermal Wnt ligands is required for fibroblast proliferation and hair follicle initiation. *Development* **139**, 1522-1533.

Corbit, K. C., Aanstad, P., Singla, V., Norman, A. R., Stainier, D. Y. R. and Reiter, J. F. (2005). Vertebrate Smoothened functions at the primary cilium. *Nature* **437**, 1018-1021.

Day, T. F., Guo, X., Garrett-Beal, L. and Yang, Y. (2005). Wnt/beta-catenin signaling in mesenchymal progenitors controls osteoblast and chondrocyte differentiation during vertebrate skeletogenesis. *Dev. Cell* **8**, 739-750.

Donnelly, E., Williams, R. and Farnum, C. (2008). The primary cilium of connective tissue cells: imaging by multiphoton microscopy. *Anat. Rec. (Hoboken)* **291**, 1062-1073.

Duboc, V. and Logan, M. P. O. (2011). Regulation of limb bud initiation and limb-type morphology. *Dev. Dyn.* **240**, 1017-1027.

Farnum, C. E. and Wilsman, N. J. (2011). Axonemal positioning and orientation in three-dimensional space for primary cilia: what is known, what is assumed, and what needs clarification. *Dev. Dyn.* **240**, 2405-2431.

Feigin, M. E., Xue, B., Hammell, M. C. and Muthuswamy, S. K. (2014). G-protein-coupled receptor GPR161 is overexpressed in breast cancer and is a promoter of cell proliferation and invasion. *Proc. Natl. Acad. Sci. USA* **111**, 4191-4196.

Glotzer, D. J., Zelzer, E. and Olsen, B. R. (2008). Impaired skin and hair follicle development in Runx2 deficient mice. *Dev. Biol.* **315**, 459-473.

Goetz, S. C. and Anderson, K. V. (2010). The primary cilium: a signalling centre during vertebrate development. *Nat. Rev. Genet.* **11**, 331-344.

Goodnough, L. H., Chang, A. T., Treloar, C., Yang, J., Scacheri, P. C. and Atit, R. P. (2012). Twist1 mediates repression of chondrogenesis by beta-catenin to promote cranial bone progenitor specification. *Development* **139**, 4428-4438.

Goodrich, L. V., Milenkovic, L., Higgins, K. M. and Scott, M. P. (1997). Altered neural cell fates and medulloblastoma in mouse patched mutants. *Science* **277**, 1109-1113.

Gros, J. and Tabin, C. J. (2014). Vertebrate limb bud formation is initiated by localized epithelial-to-mesenchymal transition. *Science* **343**, 1253-1256.

Hasson, P., Del Buono, J. and Logan, M. P. O. (2007). Tbx5 is dispensable for forelimb outgrowth. *Development* **134**, 85-92.

Haycraft, C. J., Zhang, Q., Song, B., Jackson, W. S., Detloff, P. J., Serra, R. and Yoder, B. K. (2007). Intraflagellar transport is essential for endochondral bone formation. *Development* **134**, 307-316.

Hill, T. P., Später, D., Taketo, M. M., Birchmeier, W. and Hartmann, C. (2005). Canonical Wnt/beta-catenin signaling prevents osteoblasts from differentiating into chondrocytes. *Dev. Cell* **8**, 727-738.

Huangfu, D., Liu, A., Rakeman, A. S., Murcia, N. S., Niswander, L. and Anderson, K. V. (2003). Hedgehog signalling in the mouse requires intraflagellar transport proteins. *Nature* **426**, 83-87.

Huber, C. and Cormier-Daire, V. (2012). Ciliary disorder of the skeleton. *Am. J. Med. Genet. C Semin. Med. Genet.* **160C**, 165-174.

Humke, E. W., Dorn, K. V., Milenkovic, L., Scott, M. P. and Rohatgi, R. (2010). The output of Hedgehog signaling is controlled by the dynamic association between Suppressor of Fused and the Gli proteins. *Genes Dev.* **24**, 670-682.

Jia, J., Kolterud, A., Zeng, H., Hoover, A., Teglund, S., Toftgård, R. and Liu, A. (2009). Suppressor of Fused inhibits mammalian Hedgehog signaling in the absence of cilia. *Dev. Biol.* **330**, 452-460.

Kessel, M., Balling, R. and Gruss, P. (1990). Variations of cervical vertebrate after expression of a Hox-1.1 transgene in mice. *Cell* **61**, 301-308.

Kim, H. J., Rice, D. P., Kettunen, P. J. and Thesleff, I. (1998). FGF-, BMP- and Shh-mediated signalling pathways in the regulation of cranial suture morphogenesis and calvarial bone development. *Development* **125**, 1241-1251.

Kobayashi, T., Chung, U. I., Schipani, E., Starbuck, M., Karsenty, G., Katagiri, T., Goad, D. L., Lanske, B. and Kronenberg, H. M. (2002). PTHrP and Indian hedgehog control differentiation of growth plate chondrocytes at multiple steps. *Development* **129**, 2977-2986.

Kobayashi, T., Soegiarto, D. W., Yang, Y., Lanske, B., Schipani, E., Mcmahon, A. P. and Kronenberg, H. M. (2005). Indian hedgehog stimulates periarticular chondrocyte differentiation to regulate growth plate length independently of PTHrP. *J. Clin. Invest.* **115**, 1734-1742.

Komori, T., Yagi, H., Nomura, S., Yamaguchi, A., Sasaki, K., Deguchi, K., Shimizu, Y., Bronson, R. T., Gao, Y.-H., Inada, M. et al. (1997). Targeted disruption of Cbfa1 results in a complete lack of bone formation owing to maturational arrest of osteoblasts. *Cell* **89**, 755-764.

Koziel, L., Wuelling, M., Schneider, S. and Vortkamp, A. (2005). Gli3 acts as a repressor downstream of Ihh in regulating two distinct steps of chondrocyte differentiation. *Development* **132**, 5249-5260.

Kronenberg, H. M. (2003). Developmental regulation of the growth plate. *Nature* **423**, 332-336.

Lanske, B., Karaplis, A. C., Lee, K., Luz, A., Vortkamp, A., Pirro, A., Karperien, M., Defize, L. H. K., Ho, C., Mulligan, R. C. et al. (1996). PTH/PTHrP receptor in early development and Indian hedgehog-regulated bone growth. *Science* **273**, 663-666.

Lenton, K., James, A. W., Manu, A., Brugmann, S. A., Birker, D., Nelson, E. R., Leucht, P., Helms, J. A. and Longaker, M. T. (2011). Indian hedgehog positively regulates calvarial ossification and modulates bone morphogenetic protein signaling. *Genesis* **49**, 784-796.

Lewis, P. M., Dunn, M. P., Mcmahon, J. A., Logan, M., Martin, J. F., St-Jacques, B. and Mcmahon, A. P. (2001). Cholesterol modification of sonic hedgehog is required for long-range signaling activity and effective modulation of signaling by Ptc1. *Cell* **105**, 599-612.

Li, J., Cui, Y., Xu, J., Wang, Q., Yang, X., Li, Y., Zhang, X., Qiu, M., Zhang, Z. and Zhang, Z. (2017). Suppressor of Fused restraint of Hedgehog activity level is critical for osteogenic proliferation and differentiation during calvarial bone development. *J. Biol. Chem.* **292**, 15814-15825.

Liem, K. F., Jr, Ashe, A., He, M., Satir, P., Moran, J., Beier, D., Wicking, C. and Anderson, K. V. (2012). The IFT-A complex regulates Shh signaling through cilia structure and membrane protein trafficking. *J. Cell Biol.* **197**, 789-800.

Lin, A. E., Traum, A. Z., Sahai, I., Keppler-Noreuil, K., Kukolich, M. K., Adam, M. P., Westra, S. J. and Arts, H. H. (2013). Sensenbrenner syndrome (Cranioectodermal dysplasia): clinical and molecular analyses of 39 patients including two new patients. *Am. J. Med. Genet. A* **161A**, 2762-2776.

Litingtung, Y., Dahn, R. D., Li, Y., Fallon, J. F. and Chiang, C. (2002). Shh and Gli3 are dispensable for limb skeleton formation but regulate digit number and identity. *Nature* **418**, 979-983.

Logan, M., Martin, J. F., Nagy, A., Lobe, C., Olson, E. N. and Tabin, C. J. (2002). Expression of Cre Recombinase in the developing mouse limb bud driven by a Prxl enhancer. *Genesis* **33**, 77-80.

Long, F., Zhang, X. M., Karp, S., Yang, Y. and Mcmahon, A. P. (2001). Genetic manipulation of hedgehog signaling in the endochondral skeleton reveals a direct role in the regulation of chondrocyte proliferation. *Development* **128**, 5099-5108.

Long, F., Chung, U. I., Ohba, S., Mcmahon, J., Kronenberg, H. M. and Mcmahon, A. P. (2004). Ihh signaling is directly required for the osteoblast lineage in the endochondral skeleton. *Development* **131**, 1309-1318.

Mak, K. K., Chen, M. H., Day, T. F., Chuang, P. T. and Yang, Y. (2006). Wnt/beta-catenin signaling interacts differentially with Ihh signaling in controlling endochondral bone and synovial joint formation. *Development* **133**, 3695-3707.

Malone, A. M. D., Anderson, C. T., Tummala, P., Kwon, R. Y., Johnston, T. R., Stearns, T. and Jacobs, C. R. (2007). Primary cilia mediate mechanosensing in bone cells by a calcium-independent mechanism. *Proc. Natl. Acad. Sci. USA* **104**, 13325-13330.

Minguillon, C., Nishimoto, S., Wood, S., Vendrell, E., Gibson-Brown, J. J. and Logan, M. P. O. (2012). Hox genes regulate the onset of Tbx5 expression in the forelimb. *Development* **139**, 3180-3188.

Mukhopadhyay, S. and Rohatgi, R. (2014). G-protein-coupled receptors, Hedgehog signaling and primary cilia. *Semin. Cell Dev. Biol.* **33**, 63-72.

Mukhopadhyay, S., Wen, X., Chih, B., Nelson, C. D., Lane, W. S., Scales, S. J. and Jackson, P. K. (2010). TULP3 bridges the IFT-A complex and membrane phosphoinositides to promote trafficking of G protein-coupled receptors into primary cilia. *Genes Dev.* **24**, 2180-2193.

Mukhopadhyay, S., Wen, X., Ratti, N., Loktev, A., Rangell, L., Scales, S. J. and Jackson, P. K. (2013). The ciliary G-protein-coupled receptor Gpr161 negatively regulates the Sonic hedgehog pathway via cAMP signaling. *Cell* **152**, 210-223.

Nakashima, K., Zhou, X., Kunkel, G., Zhang, Z., Deng, J. M., Behringer, R. R. and De Crombrugghe, B. (2002). The novel zinc finger-containing transcription factor osterix is required for osteoblast differentiation and bone formation. *Cell* **108**, 17-29.

Ng, J. K., Kawakami, Y., Buscher, D., Raya, A., Itoh, T., Koth, C. M., Rodriguez Esteban, C., Rodriguez-Leon, J., Garrity, D. M., Fishman, M. C. et al. (2002). The limb identity gene Tbx5 promotes limb initiation by interacting with Wnt2b and Fgf10. *Development* **129**, 5161-5170.

Nishimoto, S., Wilde, S. M., Wood, S. and Logan, M. P. O. (2015). RA acts in a coherent feed-forward mechanism with Tbx5 to control limb bud induction and initiation. *Cell Rep.* **12**, 879-891.

Norman, R. X., Ko, H. W., Huang, V., Eun, C. M., Abler, L. L., Zhang, Z., Sun, X. and Eggenschwiler, J. T. (2009). Tubby-like protein 3 (TULP3) regulates patterning in the mouse embryo through inhibition of Hedgehog signaling. *Hum. Mol. Genet.* **18**, 1740-1754.

Ocbina, P. J. R., Eggenschwiler, J. T., Moskowitz, I. and Anderson, K. V. (2011). Complex interactions between genes controlling trafficking in primary cilia. *Nat. Genet.* **43**, 547-553.

Ohuchi, H., Nakagawa, T., Yamamoto, A., Araga, A., Ohata, T., Ishimaru, Y., Yoshioka, H., Kuwana, T., Nohno, T., Yamasaki, M. et al. (1997). The mesenchymal factor, FGF10, initiates and maintains the outgrowth of the chick limb bud through interaction with FGF8, an apical ectodermal factor. *Development* **124**, 2235-2244.

Otto, F., Thornell, A. P., Crompton, T., Denzel, A., Gilmour, K. C., Rosewell, I. R., Stamp, G. W. H., Beddington, R. S. P., Mundlos, S., Olsen, B. R. et al. (1997). Cbfa1, a candidate gene for cleidocranial dysplasia syndrome, is essential for osteoblast differentiation and bone development. *Cell* **89**, 765-771.

Pal, K., Hwang, S.-H., Somatilaka, B., Badgandi, H., Jackson, P. K., Defea, K. and Mukhopadhyay, S. (2016). Smoothened determines beta-arrestin-mediated removal of the G protein-coupled receptor Gpr161 from the primary cilium. *J. Cell Biol.* **212**, 861-875.

Patterson, V. L., Damrau, C., Paudyal, A., Reeve, B., Grimes, D. T., Stewart, M. E., Williams, D. J., Siggers, P., Greenfield, A. and Murdoch, J. N. (2009). Mouse hitchhiker mutants have spina bifida, dorso-ventral patterning defects and polydactyly: identification of Tulp3 as a novel negative regulator of the Sonic hedgehog pathway. *Hum. Mol. Genet.* **18**, 1719-1739.

Platt, K. A., Michaud, J. and Joyner, A. L. (1997). Expression of the mouse Gli and Ptc genes is adjacent to embryonic sources of hedgehog signals suggesting a conservation of pathways between flies and mice. *Mech. Dev.* **62**, 121-135.

Qin, J., Lin, Y., Norman, R. X., Ko, H. W. and Eggenschwiler, J. T. (2011). Intraflagellar transport protein 122 antagonizes Sonic Hedgehog signaling and controls ciliary localization of pathway components. *Proc. Natl. Acad. Sci. USA* **108**, 1456-1461.

Rallis, C., Bruneau, B. G., Del Buono, J., Seidman, C. E., Seidman, J. G., Nissim, S., Tabin, C. J. and Logan, M. P. (2003). Tbx5 is required for forelimb bud formation and continued outgrowth. *Development* **130**, 2741-2751.

Rohatgi, R., Milenkovic, L. and Scott, M. P. (2007). Patched1 regulates hedgehog signaling at the primary cilium. *Science* **317**, 372-376.

Sakai, K. and Miyazaki, J. (1997). A transgenic mouse line that retains Cre recombinase activity in mature oocytes irrespective of the cre transgene transmission. *Biochem. Biophys. Res. Commun.* **237**, 318-324.

Sekine, K., Ohuchi, H., Fujiwara, M., Yamasaki, M., Yoshizawa, T., Sato, T., Yagishita, N., Matsui, D., Koga, Y., Itoh, N. et al. (1999). Fgf10 is essential for limb and lung formation. *Nat. Genet.* **21**, 138-141.

Sheehan, D. C. and Hrapchak, B. B. (1980). *Theory and Practice of Histotechnology*. St. Louis: Mosby.

Shelton, J. M., Lee, M. H., Richardson, J. A. and Patel, S. B. (2000). Microsomal triglyceride transfer protein expression during mouse development. *J. Lipid Res.* **41**, 532-537.

Song, B., Haycraft, C. J., Seo, H.-S., Yoder, B. K. and Serra, R. (2007). Development of the post-natal growth plate requires intraflagellar transport proteins. *Dev. Biol.* **305**, 202-216.

St-Jacques, B., Hammerschmidt, M. and Mcmahon, A. P. (1999). Indian hedgehog signaling regulates proliferation and differentiation of chondrocytes and is essential for bone formation. *Genes Dev.* **13**, 2072-2086.

Sun, X., Mariani, F. V. and Martin, G. R. (2002). Functions of FGF signalling from the apical ectodermal ridge in limb development. *Nature* **418**, 501-508.

Svärd, J., Heby-Henricson, K., Persson-Lek, M., Rozell, B., Lauth, M., Bergström, A., Ericson, J., Toftgård, R. and Teglund, S. (2006). Genetic elimination of Suppressor of fused reveals an essential repressor function in the mammalian Hedgehog signaling pathway. *Dev. Cell* **10**, 187-197.

Takarada, T., Nakazato, R., Tsuchikane, A., Fujikawa, K., Iezaki, T., Yoneda, Y. and Hinoi, E. (2016). Genetic analysis of Runx2 function during intramembranous ossification. *Development* **143**, 211-218.

Te Welscher, P., Fernandez-Teran, M., Ros, M. A. and Zeller, R. (2002a). Mutual genetic antagonism involving GLI3 and dHAND prepatterns the vertebrate limb bud mesenchyme prior to SHH signaling. *Genes Dev.* **16**, 421-426.

Te Welscher, P., Zuniga, A., Kuijper, S., Drenth, T., Goedemans, H. J., Meijlink, F. and Zeller, R. (2002b). Progression of vertebrate limb development through SHH-mediated counteraction of GLI3. *Science* **298**, 827-830.

Tran, P. V., Haycraft, C. J., Besschetnova, T. Y., Turbe-Doan, A., Stottmann, R. W., Herron, B. J., Chesebro, A. L., Qiu, H., Scherz, P. J., Shah, J. V. et al. (2008). THM1 negatively modulates mouse sonic hedgehog signal transduction and affects retrograde intraflagellar transport in cilia. *Nat. Genet.* **40**, 403-410.

Tran, T. H., Jarrell, A., Zentner, G. E., Welsh, A., Brownell, I., Scacheri, P. C. and Atit, R. (2010). Role of canonical Wnt signaling/ss-catenin via Dermo1 in cranial dermal cell development. *Development* **137**, 3973-3984.

Tuson, M., He, M. and Anderson, K. V. (2011). Protein kinase A acts at the basal body of the primary cilium to prevent Gli2 activation and ventralization of the mouse neural tube. *Development* **138**, 4921-4930.

Vortkamp, A., Lee, K., Lanske, B., Segre, G. V., Kronenberg, H. M. and Tabin, C. J. (1996). Regulation of rate of cartilage differentiation by Indian hedgehog and PTH-related protein. *Science* **273**, 613-622.

Wen, X., Lai, C. K., Evangelista, M., Hongo, J.-A., De Sauvage, F. J. and Scales, S. J. (2010). Kinetics of hedgehog-dependent full-length Gli3 accumulation in primary cilia and subsequent degradation. *Mol. Cell. Biol.* **30**, 1910-1922.

Wilsman, N. J., Farnum, C. E. and Reed-Aksamit, D. K. (1980). Incidence and morphology of equine and murine chondrocytic cilia. *Anat. Rec.* **197**, 355-361.

Xiao, Z., Zhang, S., Mahlios, J., Zhou, G., Magenheimer, B. S., Guo, D., Dallas, S. L., Maser, R., Calvet, J. P., Bonewald, L. et al. (2006). Cilia-like structures and polycystin-1 in osteoblasts/osteocytes and associated abnormalities in skeletogenesis and Runx2 expression. *J. Biol. Chem.* **281**, 30884-30895.

Yang, Y., Topol, L., Lee, H. and Wu, J. (2003). Wnt5a and Wnt5b exhibit distinct activities in coordinating chondrocyte proliferation and differentiation. *Development* **130**, 1003-1015.

Zeller, R., López-Ríos, J. and Zuniga, A. (2009). Vertebrate limb bud development: moving towards integrative analysis of organogenesis. *Nat. Rev. Genet.* **10**, 845-858.

Zhulyn, O., Li, D., Deimling, S., Vakili, N. A., Mo, R., Puviindran, V., Chen, M.-H., Chuang, P.-T., Hopyan, S. and Hui, C. C. (2014). A switch from low to high Shh activity regulates establishment of limb progenitors and signaling centers. *Dev. Cell* **29**, 241-249.

Supplementary Experimental Methods

Antibodies and Reagents

Rabbit anti-Arl13b polyclonal serum was a gift from Tamara Caspary (Caspary et al., 2007) (1:500). Commercial antibodies used were against Arl13b (mAb N295B/66, Neuromab; 1:500), Gli3 (AF3690, R&D, 1:1000), α-tubulin (clone DM1A, T6199, Sigma; 1:5000), acetylated α-tubulin (mAb 6-11B-1, Sigma; 1:2000), Gli1 (L42B10, Cell Signaling; 1:1000), FoxA2 (ab40874, Abcam; 1:2000), BrdU (11170376001, Sigma-Aldrich, Fig. 5; 1:25), BrdU (BU1/75[ICR1], Abcam, Fig. S7; 1:200), Cyclin D1 (RB9041, Thermo Scientific; 1:200), and p130 (21/p130[Cas], 610271, Becton Dickinson; 1:200). Monoclonal antibodies developed by O.D. Madsen (Nkx6.1: 1:10) were obtained from the Developmental Studies Hybridoma Bank developed under the auspices of the NICHD and maintained by the Department of Biological Sciences, the University of Iowa, Iowa City IA 52242, USA. Fluorescent secondary antibodies for immunofluorescence were from Jackson ImmunoResearch (1:2000 for Alexa488 labeled secondary antibodies, and 1:1000 for the rest), while IRDye 700CW and IRDye 800CW secondary antibodies for immunoblotting were from Li-cor Biosciences (used at 1:5000).

Primary cell culture, Reverse transcription and Quantitative PCR

The dissected forelimbs of E13.5 *Gpr161*$^{f/f}$ embryos were mechanically dissociated by pipetting, and by Trypsin-EDTA treatment. Dissociated cells were maintained in medium containing 10% FBS (high-glucose DMEM, 0.05 mg/ml penicillin, 0.05 mg/ml streptomycin, 2 mM glutamax, 0.1 mM MEM nonessential amino acid supplement, and freshly prepared 0.1 mM β-mercaptoethanol), and assayed within 4-5 passages in culture. For qRT-PCR, total RNA was prepared with GenElute mammalian total RNA purification kit (Sigma). RNA was used for qRT-PCR by using TaqMan one-step RT-PCR master mix reagents (Applied Biosystems). TaqMan probes for qRT-PCR were

published before (Wen et al., 2010) and an inventoried probe for *Gpr161* was from Applied Biosystems. Triplicate reactions were run and analyzed on an ABI 7500 thermocycler using murine *Rpl19* as the endogenous control.

Scanning EM

Embryos were fixed in ½ Karnovsky's fixative (2% PFA, 2.5% Glutaraldehyde in 0.1M Sodium Cacodylate buffer, pH 7.4) overnight and post fixed in 1% OsO_4 for 1 h. They were dehydrated through a series of ethanol. After three washes of hexamethyldesilazane, the samples were air dried at room temperature. The embryos were oriented and mounted on carbon tape on aluminum stubs. They were then sputter coated with 10 nm of gold/palladium mixture and viewed on an FEI XL30 SEM at 10 kV.

Supplementary References

CASPARY, T., LARKINS, C. E. & ANDERSON, K. V. 2007. The graded response to Sonic Hedgehog depends on cilia architecture. *Dev Cell,* 12**,** 767-78.

LOGAN, M., MARTIN, J. F., NAGY, A., LOBE, C., OLSON, E. N. & TABIN, C. J. 2002. Expression of Cre Recombinase in the developing mouse limb bud driven by a Prxl enhancer. *Genesis,* 33**,** 77-80.

RODDA, S. J. & MCMAHON, A. P. 2006. Distinct roles for Hedgehog and canonical Wnt signaling in specification, differentiation and maintenance of osteoblast progenitors. *Development,* 133**,** 3231-44.

WEN, X., LAI, C. K., EVANGELISTA, M., HONGO, J. A., DE SAUVAGE, F. J. & SCALES, S. J. 2010. Kinetics of hedgehog-dependent full-length Gli3 accumulation in primary cilia and subsequent degradation. *Mol Cell Biol,* 30**,** 1910-22.

Supplementary Figure

Fig. S1. Generation of a conditional knockout *Gpr161* allele in mice.
(A) Cartoon depicting strategy for conditional and full knockout of *Gpr161* exon 4. PCR-based genotyping for wild type, floxed (f) and knockout (-) alleles.
(B) Horizontal cryosections of *Gpr161* exon 4 heterozygote (+/-) and knockout (-/-) shows ventralization of neuroprogenitor markers FoxA2 and Nkx6.1 in lumbar neural tube at E10.25. Scale, 100 μm.
(C) Immunoblotting for Gli1 (left) and Gli3 (center) in *Gpr161* exon 4 wild type (+/+) and knockout (-/-) whole embryo lysates show increased Gli1 levels and decreased Gli3 full length (Gli3FL) and Gli3R levels when normalized to α-tubulin. qRT PCR for designated transcripts to the right. N=3 each. Data represented as mean ± SD. ***, P<0.001 **, P<0.01; *, P<0.05 by *t*-test.
(D) Primary forelimb bud mesenchymal cells cultured from E13.5 *Gpr161*$^{f/f}$ embryos were fixed after starving for 48 h. Cells were immunostained for Gpr161 (green), acetylated tub (AcTub, red), and DNA. Inset shows cilia. Arrows depict Gpr161 positive cilia, yellow arrow depicts cilia shown in inset, and arrowhead depicts cilia negative for Gpr161. Scale, 5 μm.
(E) Scanning electron micrographs of E10.25 *Gpr161* heterozygote (+/-) showing presence of both fore/hindlimb buds in lateral view (left panel), and *Gpr161* knockout (-/-) showing lack of forelimbs and presence of hindlimbs in *en face* (middle panel) and lateral view (right panel). Black arrow and white arrowheads mark forelimb and hindlimbs, respectively. White arrow marks absent forelimb. Scale, 200 μm.

Hwang_Figure S1

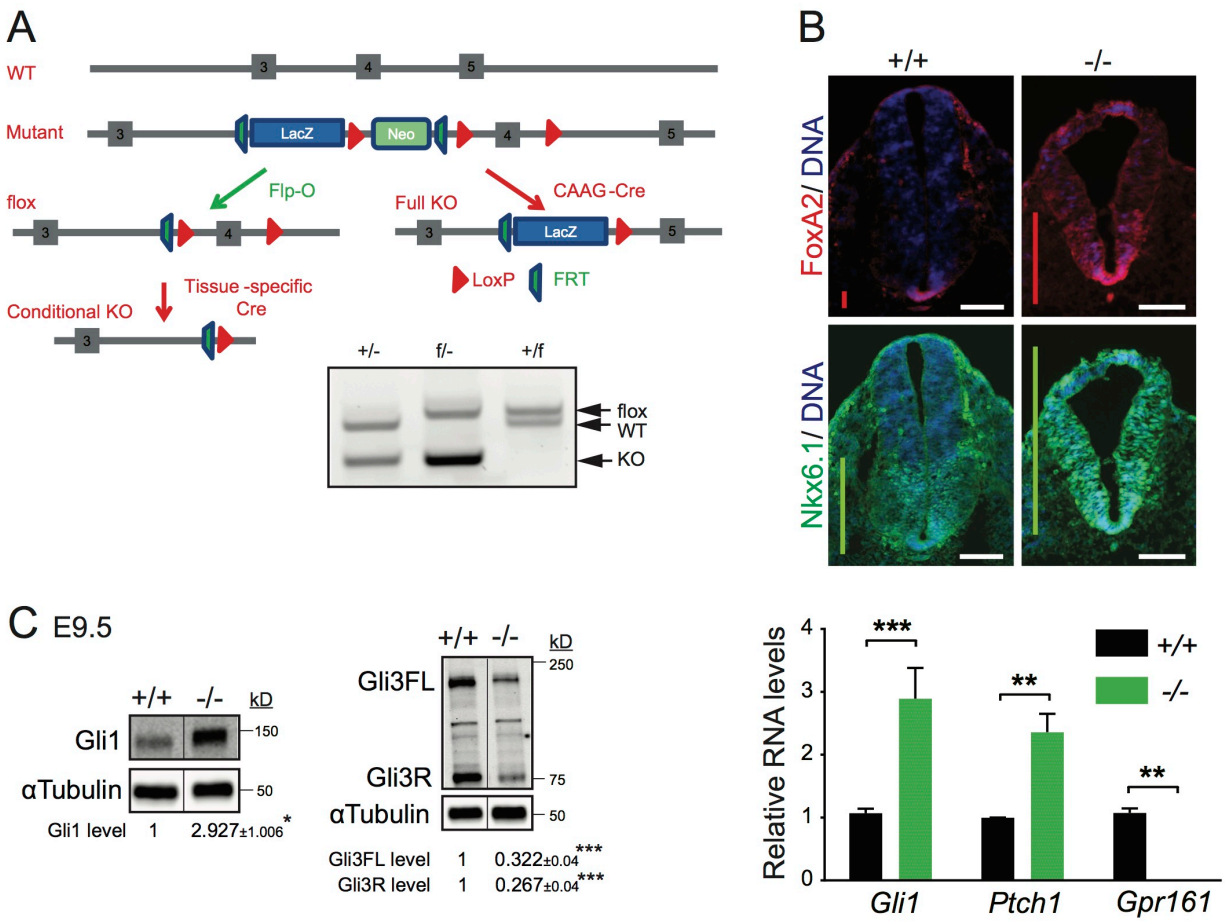

Fig. S2. *Gpr161* knockouts exhibit high Shh pathway activity.
(A) Whole-mount digoxigenin-labeled RNA in situ hybridization for *Gli3* show similar expression in anterior forelimb buds in control littermate (WT) and *Prx1-Cre; Gpr161*$^{f/f}$ (cko) embryos before *Shh* expression at E9.5. Limb buds are depicted by white arrows. N=4 (WT; *Prx1-Cre; Gpr161*$^{f/+}$) and 5 (cko) embryos each.
(B) Whole-mount digoxigenin-labeled RNA in situ hybridization for *Ptch1* and *Shh* show normal expression in E10.5 hindlimb buds of *Prx1-cre; Gpr161*$^{f/+}$ (WT) versus *Prx1-cre; Gpr161*$^{f/f}$ (cko) embryos. By E10.75, *Hoxd13* expression is anteriorly expanded in hindlimb buds in cko embryos. Abbreviations: A, anterior; P, posterior. N=4 limbs each. Scale, 500 μm (A); 200 μm (B).

Hwang_Figure S2

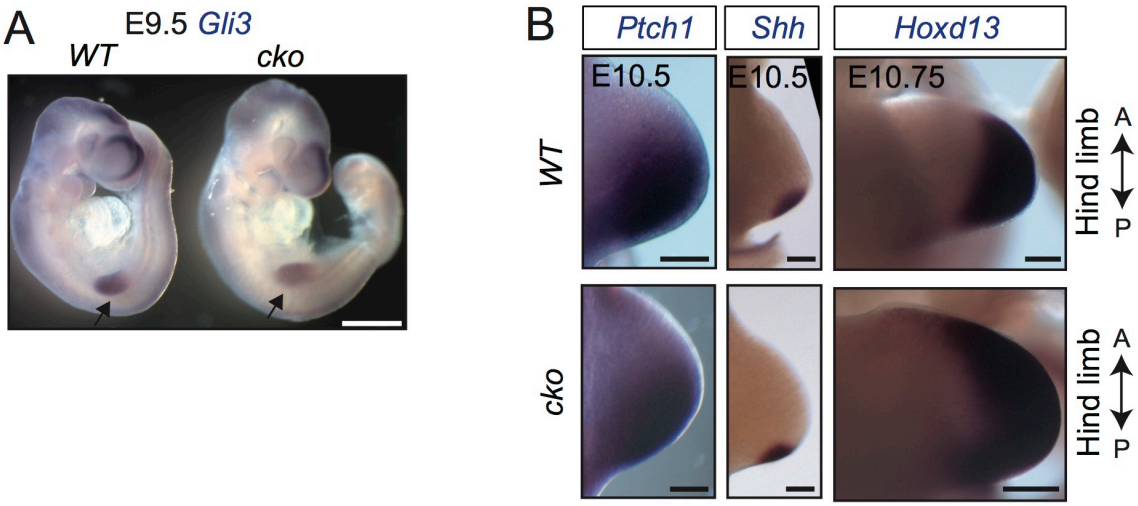

Fig. S3. Gpr161 determines endochondral and intramembranous bone formation.
(A) *Prx1-cre; Rosa26-loxP-STOP-loxP-tdTomato* (*Rosa-LSL-tdT*) embryos depict tdTomato positive fore/hindlimb buds and cranial mesenchyme (arrowhead) (Logan et al., 2002). All lateral views, except right panel (*en face*). Scale, 1 mm.
(B) Alcian blue and alizarin red staining of E16.5 forelimbs (bottom view, left; side view, right) in *Prx1-cre; Gpr161*$^{f/f}$ (*Gpr161* cko) (N=19) shows complete lack of mineralization in humerus (h), radius (r) and ulna (u). Scale, 2 mm.
(C) Horizontal sections from E18.5 *Prx1-cre; Gpr161*$^{f/+}$ (WT) and *Prx1-cre; Gpr161*$^{f/f}$ (*Gpr161* cko) at thoracic level (left two panels) and at abdominal level (right two panels) show ribcage lacking ventral rib fusion, anterior abdominal wall defects, and protruding internal organs in *Gpr161* cko. Scale, 2 mm.
(D) Alcian blue and alizarin red staining of base of the skull from E18.5 of (i) *Prx1-Cre; Gpr161*$^{f/+}$ (WT) (N=20) and (ii) *Prx1-Cre; Gpr161*$^{f/f}$ (*Gpr161* cko) (N=19), show intact endochondral bones in the base of the skull. Abbreviations: bo, basiocciput; bs, basisphenoid; ps, presphenoid.

Hwang_Figure S3

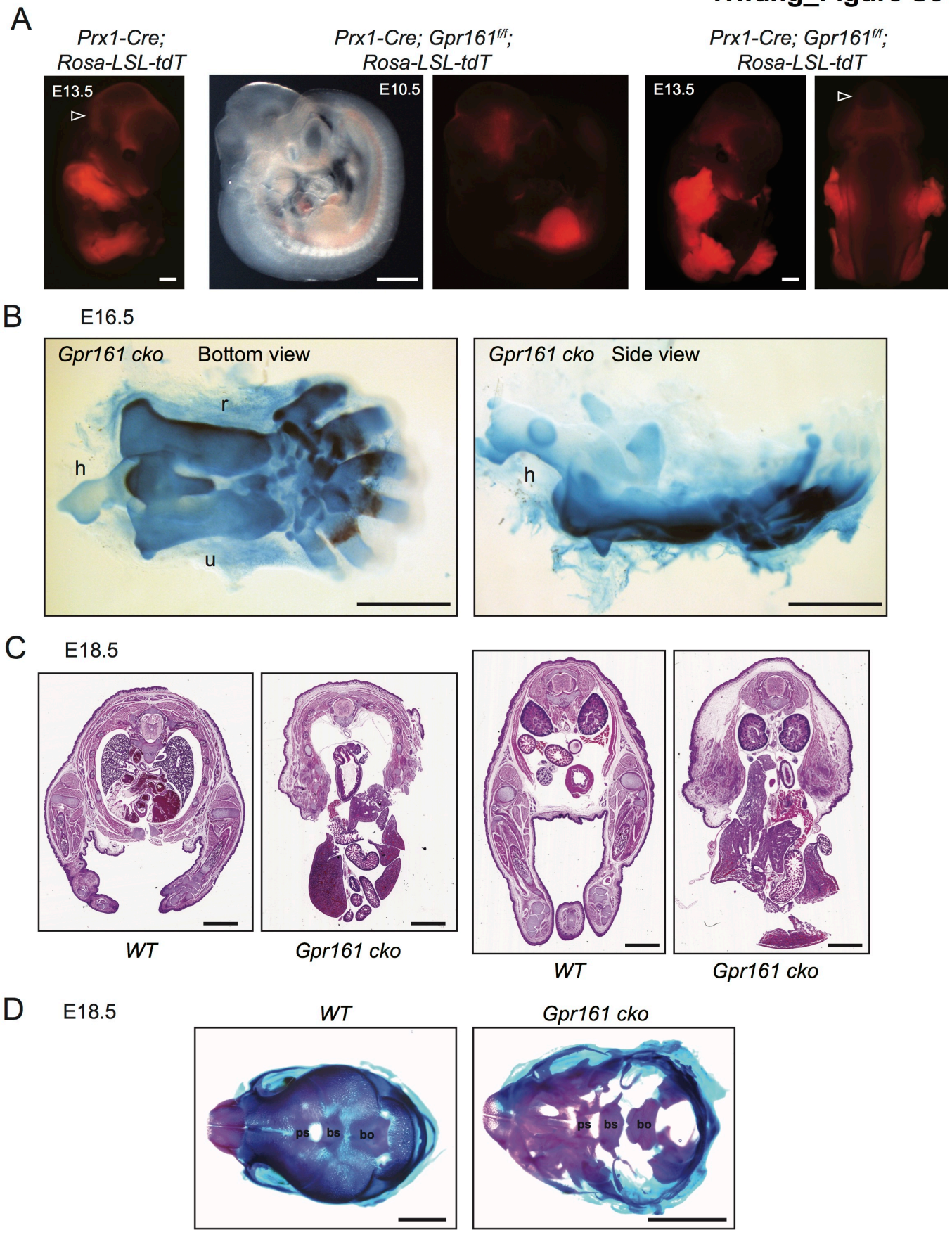

Fig. S4. Lack of maturation and sustained proliferation of periarticular/round chondrocytes in *Gpr161* cko.
(A) Magnified regions of designated region " c "or " c' " from the *Prx1-cre; Gpr161$^{f/f}$* (cko) ulna stained by Safranin O, and von Kossa. Only a few columnar and hypertrophic chondrocytes are visible. Serial sections of this region show faint Ihh expression (Fig. 6A).
(B) E14.5 *Prx1-cre; Gpr161$^{f/+}$* (WT) and *Prx1-cre; Gpr161$^{f/f}$* (cko) forearm cryosections were immunostained for Cyclin D1 (green) and p130 (red). Proximal radius for WT and the whole extent of long bone in cko zeugopod is shown. Note that proliferating chondrocytes in cko are Cyclin D1 positive and lack p130. N=3 each. Scale, 100 μm.
(C) E17.5 *Prx1-cre; Gpr161$^{f/+}$* (WT) (N=1) and (ii) *Prx1-cre; Gpr161$^{f/f}$* (cko) (N=2) hindlimbs sectioned horizontally were stained by Safranin O (left), and von Kossa (right). Note lack of ossification in tibia in *Gpr161* cko (bracket/asterisk). Scale, 1 mm.

Hwang_Figure S4

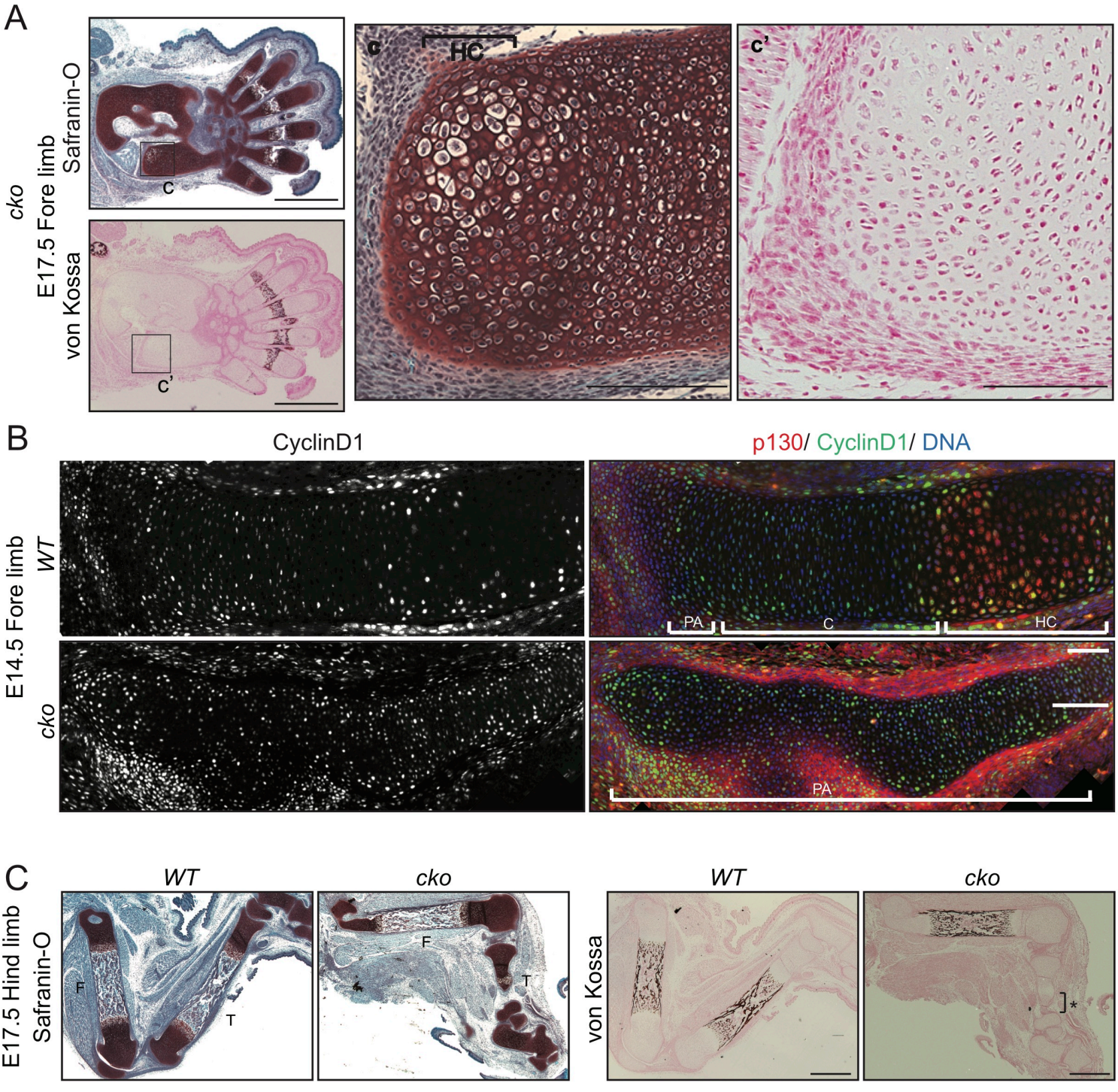

Fig. S5. Decreased Ihh signaling in *Gpr161* cko.
(A) Steps in chondrogenesis and osteogenesis, and role of Ihh signaling during endochondral bone morphogenesis (Rodda and McMahon, 2006).
(B) Full forearm including autopods as shown in Fig. 6A. Note that adjacent autopod metacarpals exhibit Ihh targets *Ptch1* and *Gli1* (perichondrium and proliferating chondrocytes), *Ihh* (prehypertrophic and hypertrophic chondrocytes), *Col X* (hypertrophic chondrocytes), *Runx2* (osteoblast progenitors) and *Osx* (immature osteoblasts). Skin hair follicles also exhibit Shh pathway activation (*Ptch1*, *Gli1* expression). Abbreviations: R, radius; U, ulna. Scale, 1 mm.
(C) Embryos sectioned horizontally at forelimb levels from (i) *Prx1-Cre; Gpr161*$^{f/+}$ (WT) (N=2 sides) and (ii) *Prx1-Cre; Gpr161*$^{f/f}$ (cko) (N=8 sides), with designated insets as shown in Fig. 6B.
(D) E17.5 (i) *Prx1-cre; Gpr161*$^{f/+}$ (WT) (N=1) and (ii) *Prx1-cre; Gpr161*$^{f/f}$ (cko) (N=2) hindlimbs sectioned horizontally were probed for expression of designated transcript levels as in Fig. 6. Note that hindlimbs of *Gpr161* cko were less or not affected as in forelimbs (Fig. 6). Abbreviations: F, femur; T, tibia; Fi, fibula. Scale; 1mm.

Hwang_Figure S5

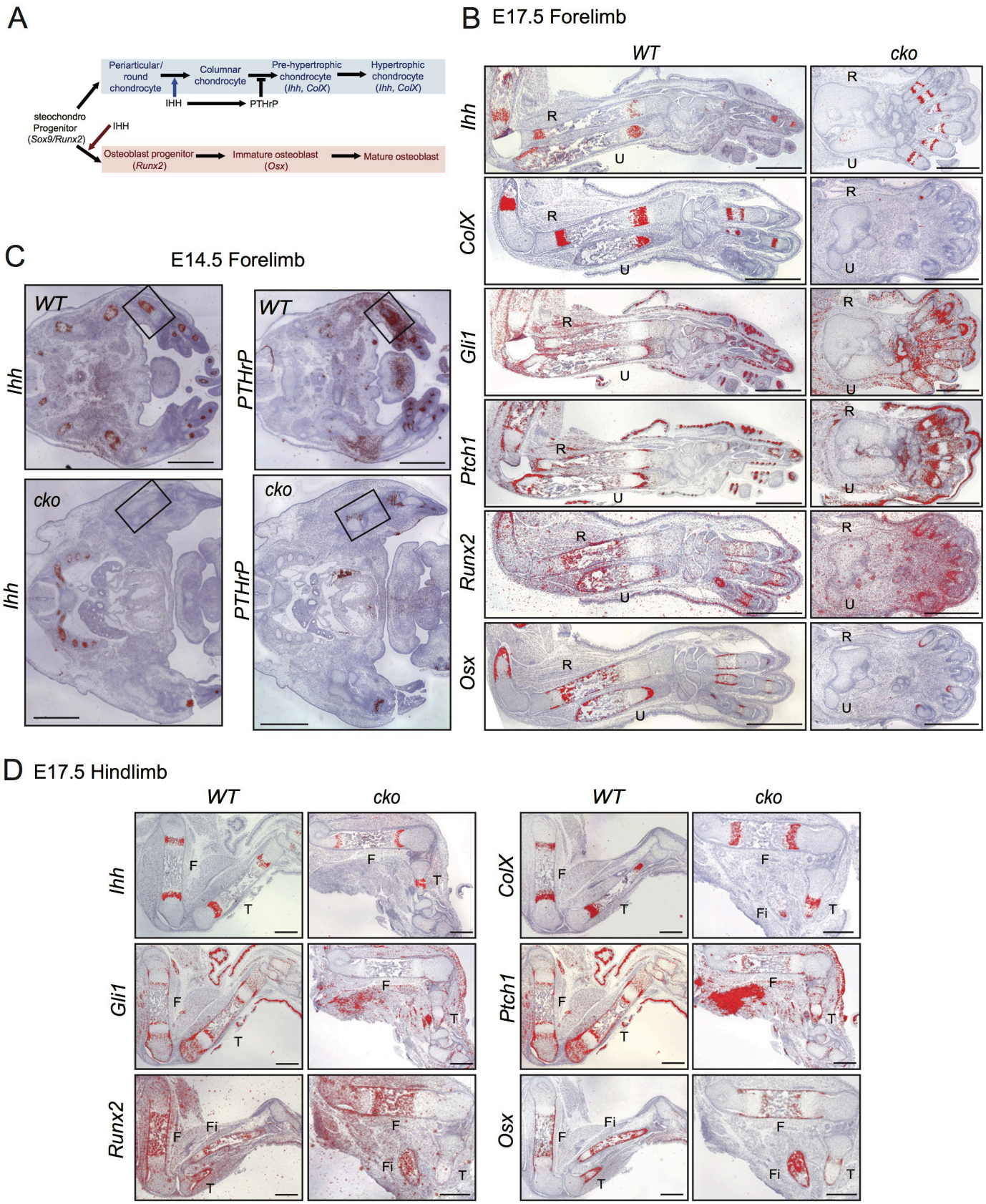

Fig. S6. Gpr161 determines limb patterning and skeletogenesis in a cilia-dependent manner.

(A) Designated regions in sections consecutive to HE stained sections (left) from P0 *Prx1-Cre; Gpr161*$^{f/+}$ (WT), *Gpr161 Ift88* dko, and *Ift88* cko forelimbs were quantified for Arl13b+ cilia after immunostaining for Arl13b (red) and DNA (blue). Arrows refer to cilia. Quantification to the right. N=3 sections each. Data represented as mean ± SD. Scale, 1 mm (left HE panel), 10 μm (right panels). Abbreviations: PA, periarticular/round chondrocytes; CC, columnar chondrocytes; HC, hypertrophic chondrocytes.

(B) Designated regions from E17.5 *Prx1-cre; Gpr161*$^{f/+}$ (WT) and *Prx1-cre; Gpr161*$^{f/f}$ (cko) forearm cryosections were immunostained for BrdU (3 h pre-labeled before harvesting embryos) (magenta), and Arl13b (green). Note that proliferating chondrocytes in cko are ciliated, irrespective of BrdU labeling. Arrows and arrowheads refer to BrdU +ve ciliated cells and BrdU -ve ciliated cells, respectively. N=3 each. Scale, 100 μm (left), 10 μm (right).

(C) Designated regions similar to **(B)** from E14.5 *Prx1-cre; Gpr161*$^{f/+}$ (WT) and *Prx1-cre; Gpr161*$^{f/f}$ (cko) forearm cryosections were immunostained for Cyclin D1 (green) and Arl13b (red). Note that proliferating chondrocytes in cko are ciliated, irrespective of Cyclin D1 labeling. Arrows and arrowheads refer to cyclin D1 +ve ciliated cells and cyclin D1 -ve ciliated cells, respectively. N=2 each. Scale, 10 μm.

Hwang_Figure S6

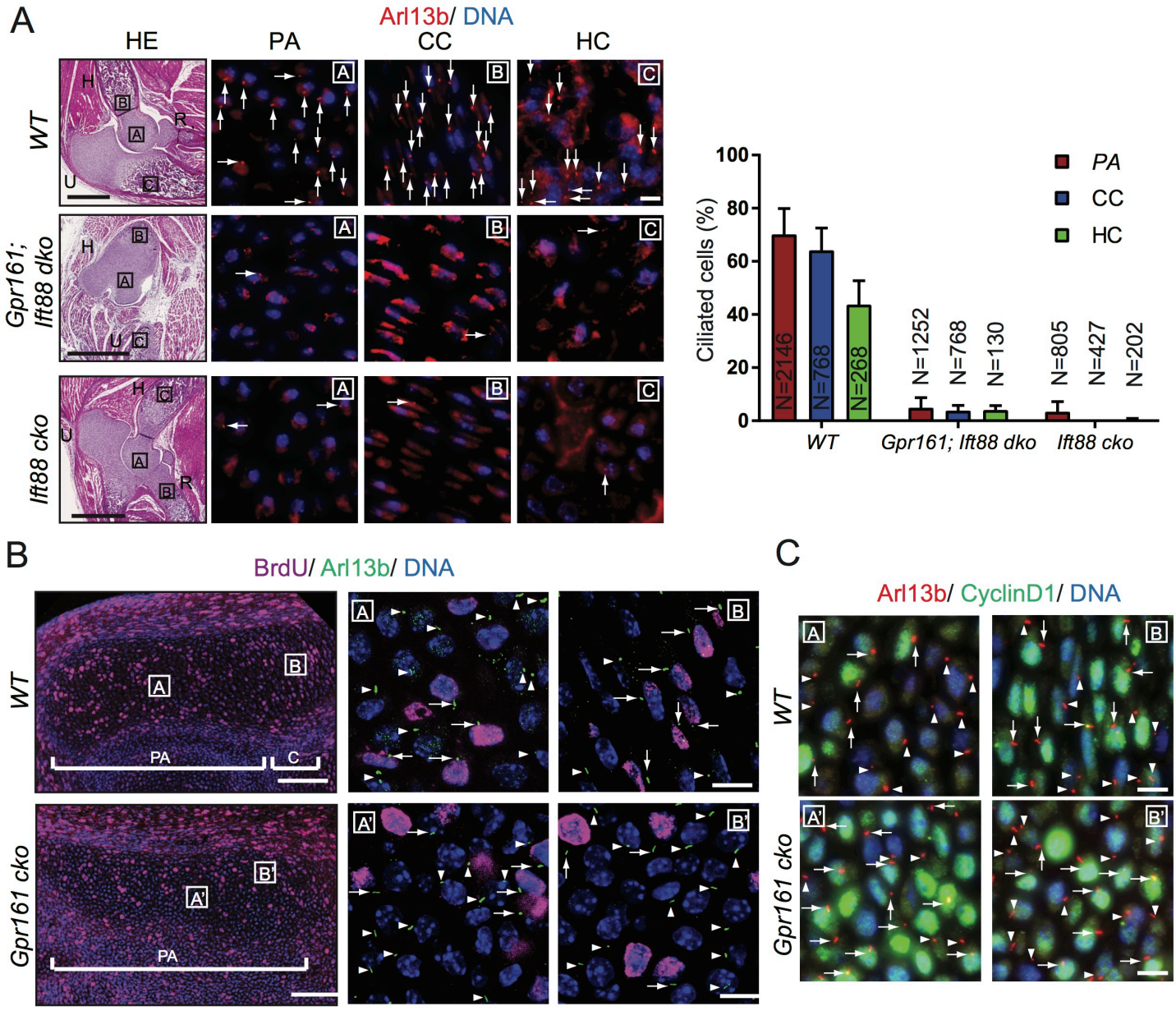

Supplementary Movies

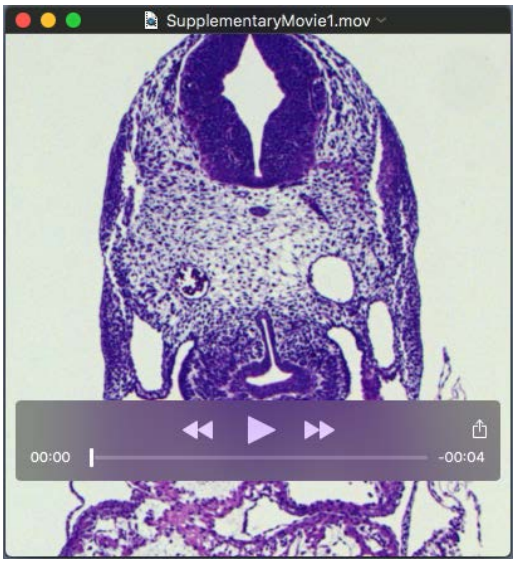

Movie 1. Forelimb buds in wild type embryo at E10.25. Paraffin sections were made at 5 μm thickness starting from the cardiac level and collected every 30 μm for hematoxylin and eosin staining, along with 5 more serial sections for mounting to unstained slides. Serial sections show forelimb mesenchyme. Orientation of embryo section as in Figure 1B.

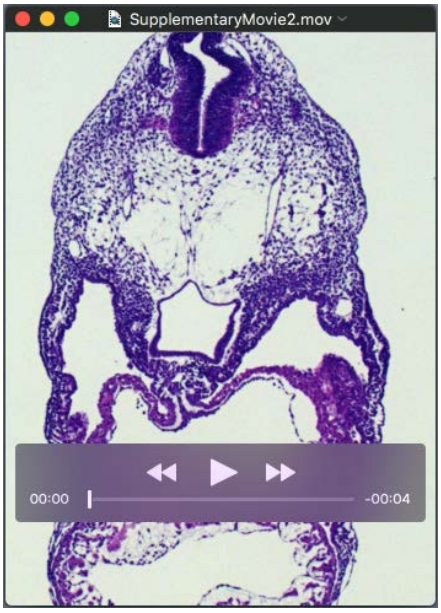

Movie 2. Lack of forelimbs in *Gpr161*$^{-/-}$ embryo at E10.25. Serial sections collected and processed as in Movie 1 starting from the cardiac level show lack of forelimb mesenchyme. Orientation of embryo section as in Figure 1B'.

Movie 3. Hindlimb buds in wild type embryo at E10.25. Serial sections collected and processed as in Movie 1 starting from the lumbar level show hindlimb bud. Later caudal sections are missing in the video. Orientation of embryo section as in Figure 1B.

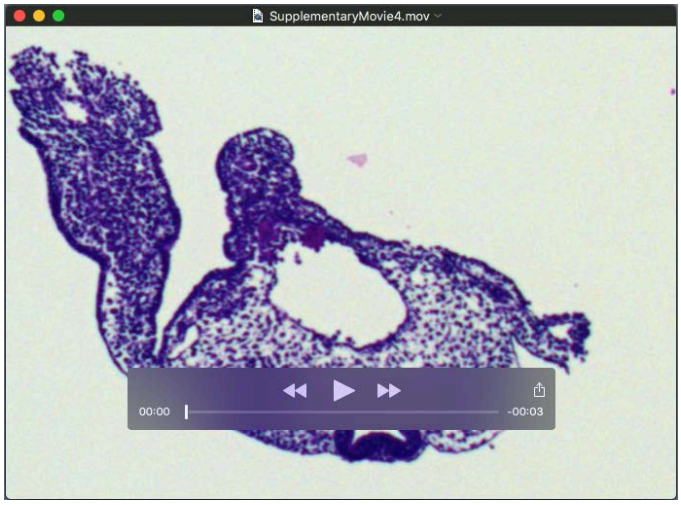

Movie 4. Hindlimb buds in *Gpr161*$^{-/-}$ embryo at E10.25. Serial sections collected and processed as in Movie 1 starting from the lumbar level show hindlimb bud. Later caudal sections with open neural tube are missing in the video. Orientation of embryo section as in Figure 1B'.